A&A 587, A68 (2016)
DOI: 10.1051/0004-6361/201527795

Astronomy & Astrophysics

Spectacular tails of ionized gas in the Virgo cluster galaxy NGC 4569⋆,⋆⋆

A. Boselli[1], J. C. Cuillandre[2], M. Fossati[3,4], S. Boissier[1], D. Bomans[5], G. Consolandi[6], G. Anselmi[7], L. Cortese[8], P. Côté[9], P. Durrell[10], L. Ferrarese[9], M. Fumagalli[11], G. Gavazzi[6], S. Gwyn[9], G. Hensler[12,13], M. Sun[14], and E. Toloba[15,16]

[1] Aix Marseille Université, CNRS, LAM (Laboratoire d'Astrophysique de Marseille), UMR 7326, 13388 Marseille, France
e-mail: alessandro.boselli@lam.fr
[2] CEA/IRFU/SAP, Laboratoire AIM Paris-Saclay, CNRS/INSU, Université Paris Diderot, Observatoire de Paris, PSL Research University, 91191 Gif-sur-Yvette Cedex, France
[3] Universitäts-Sternwarte München, Scheinerstrasse 1, 81679 München, Germany
[4] Max-Planck-Institut für Extraterrestrische Physik, Giessenbachstrasse, 85748 Garching, Germany
[5] Astronomical Institute of the Ruhr-Universität Bochum, Universitätsstr. 150, 44801 Bochum, Germany
[6] Universitá di Milano-Bicocca, piazza della scienza 3, 20100 Milano, Italy
[7] Coelum Astronomia, via Appia 20, 30173 Venezia, Italy
[8] International Centre for Radio Astronomy Research, The University of Western Australia, 35 Stirling Highway, Crawley WA 6009, Australia
[9] NRC Herzberg Astronomy and Astrophysics, 5071 West Saanich Road, Victoria, BC, V9E 2E7, Canada
[10] Department of Physiscs and Astronomy, Youngstown State University, Youngstown, OH 44503, USA
[11] Institute for Computational Cosmology and Centre for Extragalactic Astronomy, Department of Physics, Durham University, South Road, Durham DH1 3LE, UK
[12] Department of Astrophysics, University of Vienna, Türkenschanzstrasse 17, 1180 Vienna, Austria
[13] National Astronomy Observatory of Japan, 2-21-1 Osawa, Mitaka-shi, 181-8588 Tokyo, Japan
[14] Physics Department, University of Alabama in Huntsville, Huntsville, AL 35899, USA
[15] UCO/Lick Observatory, University of California, Santa Cruz, 1156 High Street, Santa Cruz, CA 95064, USA
[16] Texas Tech University, Physics Department, Box 41051, Lubbock, TX 79409-1051, USA

Received 20 November 2015 / Accepted 18 January 2016

ABSTRACT

Using MegaCam at the CFHT, we obtained a deep narrow band Hα+[NII] wide-field image of NGC 4569 (M90), the brightest late-type galaxy in the Virgo cluster. The image reveals the presence of long tails of diffuse ionized gas, without any associated stellar component extending from the disc of the galaxy up to ≃80 kpc (projected distance) and with a typical surface brightness of a few 10^{-18} erg s^{-1} cm^{-2} arcsec^{-2}. These features provide direct evidence that NGC 4569 is undergoing a ram-presure stripping event. The image also shows a prominent 8 kpc spur of ionized gas that is associated with the nucleus that spectroscopic data identify as an outflow. With some assumptions on the 3D distribution of the gas, we use the Hα surface brightness of these extended low-surface brightness features to derive the density and the mass of the gas that has been stripped during the interaction of the galaxy with the intracluster medium. The comparison with ad hoc chemo-spectrophotometric models of galaxy evolution indicates that the mass of the Hα emitting gas in the tail is a large fraction of that of the cold phase that has been stripped from the disc, suggesting that the gas is ionized within the tail during the stripping process. The lack of star-forming regions suggests that mechanisms other than photoionization are responsible for the excitation of the gas (shocks, heat conduction, magneto hydrodynamic waves). This analysis indicates that ram pressure stripping is efficient in massive ($M_{\rm star} \simeq 10^{10.5}$ $M_\odot$) galaxies located in intermediate-mass ($\simeq 10^{14}$ $M_\odot$) clusters under formation. It also shows that the mass of gas expelled by the nuclear outflow is only ∼1% than that removed during the ram pressure stripping event. Together these results indicate that ram pressure stripping, rather than starvation through nuclear feedback, can be the dominant mechanism that is responsible for the quenching of the star formation activity of galaxies in high density environments.

Key words. galaxies: individual: NGC 4569 – galaxies: clusters: general – galaxies: clusters: individual: Virgo – galaxies: evolution – galaxies: interactions – galaxies: ISM

⋆ Based on observations obtained with MegaPrime/MegaCam, a joint project of CFHT and CEA/DAPNIA, at the Canadian-French-Hawaii Telescope (CFHT) which is operated by the National Research Council (NRC) of Canada, the Institut National des Sciences de l'Univers of the Centre National de la Recherche Scientifique (CNRS) of France and the University of Hawaii.

⋆⋆ The images analysed in this work are available as FITS files at the CDS via anonymous ftp to cdsarc.u-strasbg.fr (130.79.128.5) or via http://cdsarc.u-strasbg.fr/viz-bin/qcat?J/A+A/587/A68

1. Introduction

The environment plays a fundamental role in galaxy evolution. Since the early works of Hubble & Humason (1931), Abell (1965), and Oemler (1974), it has become evident that galaxies in rich environments are systematically different from those located in the field. Quiescent objects (ellipticals and lenticulars) are dominating high-density regions, such as clusters and compact groups, while late-type systems are mostly located in the field (Dressler 1980; Binggeli et al. 1988; Whitmore et al. 1993; Dressler et al. 1997). It has also become clear that the physical properties of star-forming systems that inhabit rich environments, which are characterised by a reduced atomic (e.g. Cayatte et al. 1990; Solanes et al. 2001; Vollmer et al. 2001; Gavazzi et al. 2006a) and molecular gas content (Fumagalli et al. 2009; Boselli et al. 2014c), dust content (Cortese et al. 2010; 2012a), and star formation (e.g. Kennicutt 1983; Gavazzi et al. 1998, 2006b, 2013; Lewis et al. 2002; Goto et al. 2003; Boselli et al. 2015), are systematically different from those of their isolated analogues.

As reviewed in Boselli & Gavazzi (2006), several physical mechanisms have been proposed to explain the origin of these differences. These processes belong to two main families, those related to the gravitational interactions between galaxies or with the potential well of the over dense region (tidal interactions – Merritt 1983; Byrd & Valtonen 1990; harassment – Moore et al. 1998), and those exerted by the hot and dense intracluster medium on galaxies that move at high velocity within the cluster (ram pressure stripping – Gunn & Gott 1972; viscous stripping – Nulsen 1982; thermal evaporation – Cowie & Songaila 1977; starvation – Larson et al. 1980). Since these large dynamically-bounded structures observed in the local universe form through the accretion of smaller groups of galaxies, these processes might have started to act well before galaxies entered rich clusters (pre-processing; Dressler 2004).

The identification and the physical understanding of the dominant process affecting galaxies in rich environments at different epochs is fundamental for tuning cosmological models of galaxy evolution. At present, observations and simulations give discordant results whenever large statistical samples that have been extracted from blind surveys are compared to targeted observations of nearby clusters and groups. Most hydrodynamic cosmological simulations suggest that the environmental quenching of the star formation is mainly regulated by starvation. Once in high-density regions, galaxies lose their hot gas halo during the dynamical interaction with the hostile environment. Active galactic nuclei (AGN) and supernovae feedback becomes particularly efficient in ejecting the gas out from the galactic disc, quenching the activity of star formation after several Gyr (McGee et al. 2009; Weinmann et al. 2010). This scenario is supported by the analysis of Sloan Digital Sky Survey (SDSS) data, which suggests a quenching timescale of ∼5 Gyr for galaxies in dense environments (Wetzel et al. 2012, 2013). It is also supported by the observations of several clusters at intermediate redshift (e.g. Haines et al. 2013, 2015). In its current form, however, this scenario over-predicts the number of red dwarf galaxies compared to what is observed in nearby clusters (Kang & van den Bosch 2008; Font et al. 2008; Kimm et al. 2009; De Lucia 2011; Weinmann et al. 2011; Taranu et al. 2014). At the same time chemo-spectrophotometric multizone models of starvation fail to reproduce the observed radial profiles of the cold gas and of the young stars of star forming galaxies in nearby clusters (Boselli et al. 2006).

Recent hydrodynamic simulations of individual galaxies indicate ram pressure as a compelling alternative process to explain the observed peculiarities of cluster members (Roediger & Bruggen 2007, 2008; Tonnesen & Bryan 2009, 2010, 2012). These simulations show that, whenever the different gas phases are properly simulated at high resolution, ram pressure is the dominant mechanism responsible for the gas stripping and for the following quenching of star formation in galaxies located up to ∼1 virial radius of the cluster. The recent observation of several late-type galaxies with long tails of gas without any associated stellar component at large clustercentric distances seems to corroborate this scenario (e.g. Scott et al. 2012; Yagi et al. 2010; Fossati et al. 2012). However, it remains unclear what the contribution of the nuclear feedback is to the stripping process, in particular in massive spiral galaxies where both the gravitational potential well and the nuclear activity are maximal. To date, the direct observations of the feedback process in clusters is still limited to a few central early-type galaxies with cooling flows (Fabian 2012). We, therefore, urgently need to understand the role of feedback in the environmental quenching of the star formation activity of late-type systems.

A full understanding of the gas stripping process in high-density regions requires the comparison of multifrequency observations that cover the different phases of the interstellar medium (ISM; atomic and molecular, ionised, hot gas, dust) and the different stellar populations with tuned chemo-spectrophotometric and hydrodynamic models of gas stripping. This comparison has been done in the Virgo cluster (Boselli et al. 2014b), the closest concentration of galaxies to the Milky Way (17 Mpc, Gavazzi et al. 1999; Mei et al. 2007), where multifrequency data that covers the whole electromagnetic spectrum are now available, including the dwarf galaxy population (GUViCS, Boselli et al. 2011; NGVS, Ferrarese et al. 2012; HeViCS, Davies et al. 2010; ALFALFA, Giovanelli et al. 2005). These works consistently indicate ram pressure as the dominant process responsible for the gas stripping and the quenching of the star formation activity of star-forming systems that have recently been accreted by the cluster (Cayatte et al. 1990; Solanes et al. 2001; Gavazzi et al. 2013; Boselli et al. 2008ab, 2014b). The Virgo cluster has another major quality: owing to its proximity, the angular resolution of multifrequency data is comparable to that obtained in high-resolution simulations. The comparison of the kinematic and spectrophotometric properties of several bright Virgo galaxies has indeed been crucial for the identification of the perturbing process (Vollmer et al. 1999, 2000, 2004, 2005, 2006, 2008a, 2008b, 2009, 2012; Vollmer 2003; Kenney et al. 2004; Boselli et al. 2005, 2006; Crowl & Kenney 2008; Abramson et al. 2011; Kenney et al. 2014; Abramson & Kenney 2014; Cortes et al. 2015).

A representative case is NGC 4569, the most massive late-type galaxy of the cluster ($M_* \simeq 10^{10.5}\ M_\odot$), which is located at ∼1.7 degree north-east from M 87 (corresponding to 0.32 virial radii $R_{\rm vir}$ from the cluster core, see Fig. 1). The study of the kinematic properties of the galaxy derived from HI data, combined with simulations, suggests that the galaxy has undergone a ram pressure stripping event with a peak of efficiency ∼300 Myr ago (Vollmer et al. 2004). A similar result (∼100 Myr) has been obtained by comparing the observed radial truncation of the different gaseous and stellar components with multizone chemo-spectrophotometric models of galaxy evolution that are tailored to take the effects of ram pressure and starvation into account (Boselli et al. 2006; Crowl & Kenney 2008). This galaxy, however, like most of the massive galaxies in the nearby universe, is also characterised by a nuclear activity with an associated

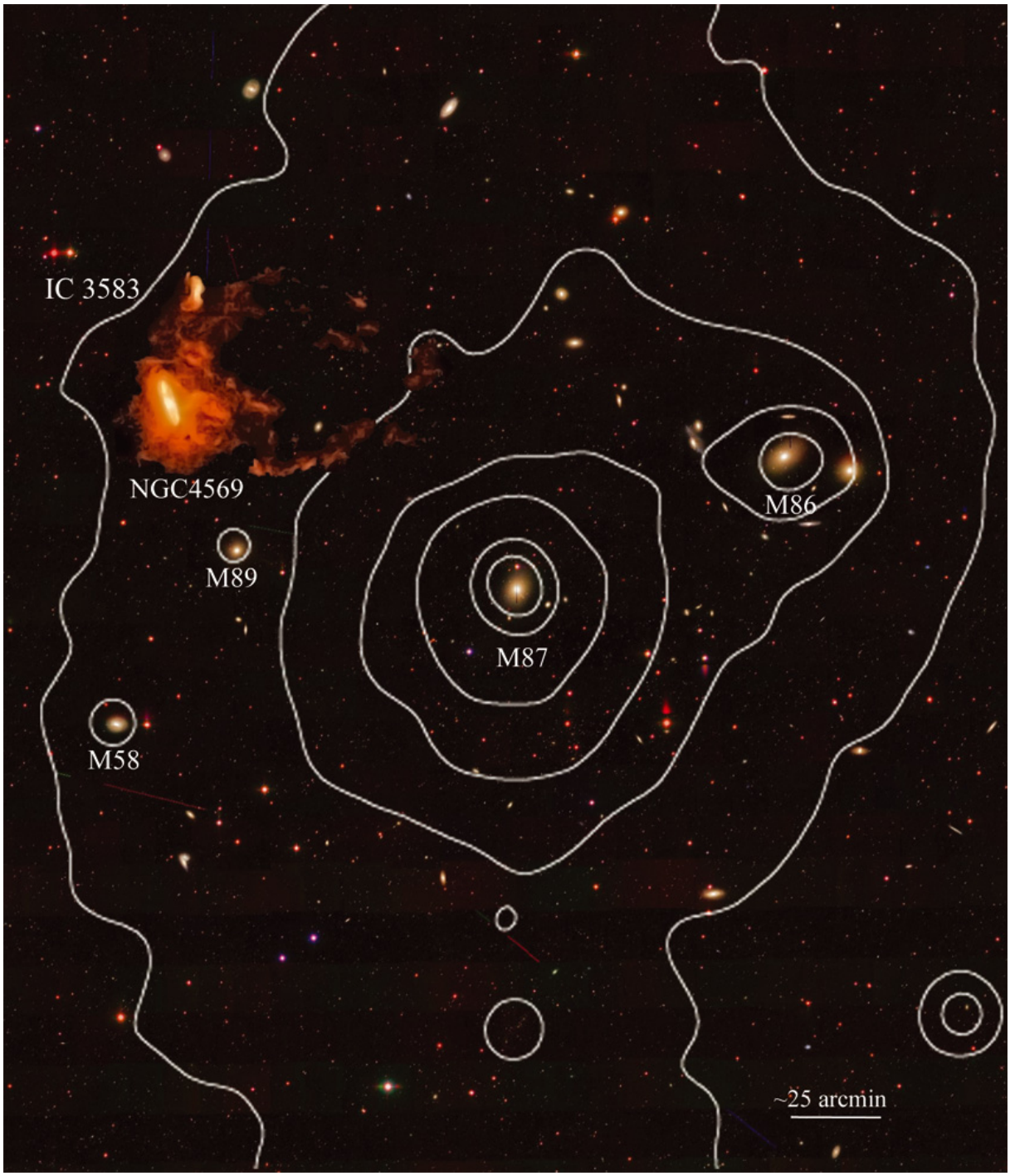

Fig. 1. Galaxy NGC 4569 is located at 1.7 degrees (0.32 R_{vir}) north-east of the core of the Virgo cluster M 87. Contours indicate the distribution of the X-ray gas as derived from ROSAT observations (Böhringer et al. 1994). The CFHT MegaCam continuum-subtracted Hα+[NII] image of the galaxy, smoothed with a 5 × 5 median filter and masked from the emission of foreground stars (see Sect. 3), is magnified by a factor of 6 to emphasise the orientation of the tail of ionized gas with respect to the position of the galaxy within the cluster.

outflow of gas (see Sect. 6.2). It is thus an ideal candidate to study the relative contribution of ram pressure stripping and nuclear feedback to the stripping process of cluster galaxies. For this purpose we obtained a deep narrow band Hα+[NII] image of NGC 4569 and its surrounding regions with MegaCam at the CFHT, which we combine here with an unpublished long-slit spectrum obtained at Calar Alto in 2001. Deep Hα imaging is used to search for long tails of ionized gas, the most direct evidence of an ongoing ram pressure stripping event (e.g. Gavazzi et al. 2001). At the same time, the impact of feedback can be quantified by studying the properties of the ionized gas that is associated with the nuclear outflow.

2. Observations

2.1. Narrow-band imaging

The observations were carried out in May 2015 using MegaCam at the CFHT. The galaxy NGC 4569, which has a recessional velocity of −221 km s^{-1}, was observed in the narrow-band filter

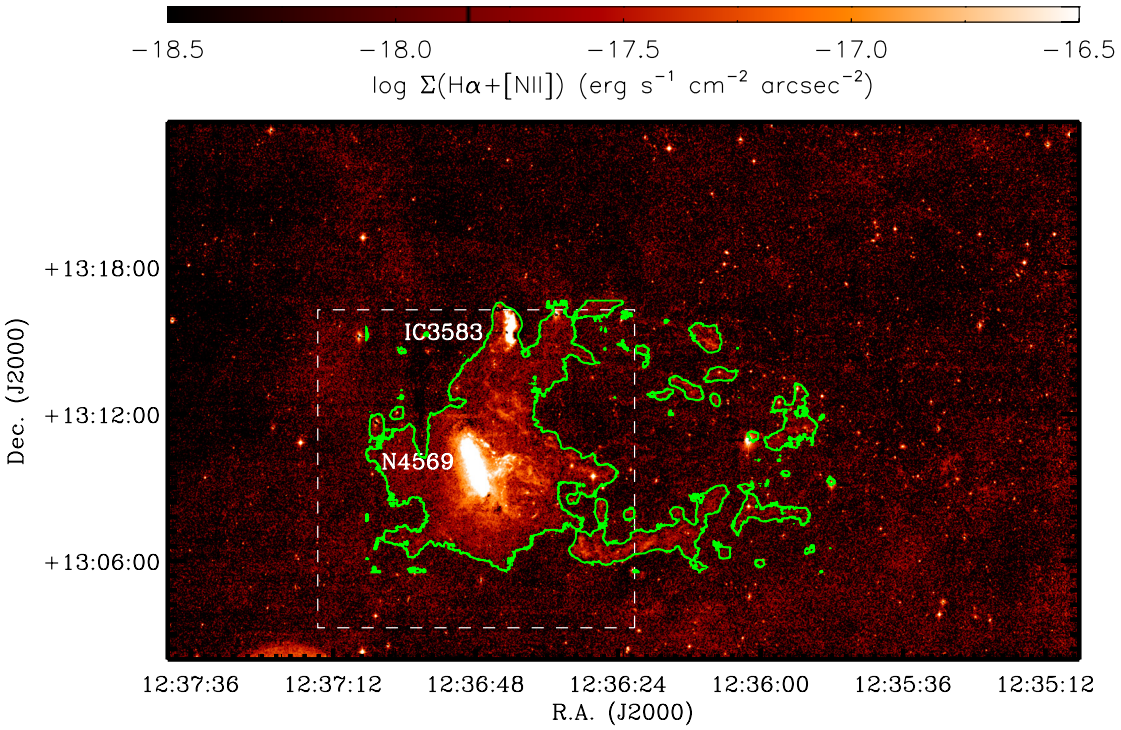

Fig. 2. CFHT MegaCam continuum-subtracted Hα+[NII] image of NGC 4569 and IC 3583 smoothed with a 5×5 median filter and masked from the emission of foreground stars. Contours are drawn from the 10^{-18} erg s^{-1} cm^{-2} arcsec^{-2} Hα+[NII] surface brightness level. The white box shows the area observed with the 1.2 m OHP telescope, as shown in Fig. 3.

MP9603 that was centered on the Hα line (λ = 6590 Å; $\Delta\lambda$ = 104 Å, T = 93%). The transmissivity T of the filter ($-1140 < vel < 3600$ km s^{-1}) perfectly covers the range in recessional velocity of the whole Virgo cluster region (Binggeli et al. 1993; Boselli et al. 2014a). Because of its width, the filter encompasses the two [NII] lines at λ = 6548 and 6584 Å. The stellar continuum was measured through the broadband r filter. Since the purpose of the present observations was to detect low surface brightness features associated with the galaxy, the observations were performed using the pointing macro QSO LDP-CCD7 optimised for Elixir-LSB observing and processing mode (see Sect. 3). This macro made seven different pointings around the galaxy using a large dithering as generally done in near-infrared imaging of extended sources. The final fully co-added image covers the central $40' \times 30'$ at maximum depth, while a larger area is mapped at lower sensitivity. This mode has been extensively used in recent years and applies well to narrow-band imaging data with long exposures (medium sky background levels). Integration times were of 660 s per pointing in the ON-band image, and 66 s in the OFF-band r-band filter, thus the resulting integration time on the stacked image is of 4620 s in Hα+[NII] and 462 s in r. The photometric calibration of the data, taken in photometric conditions, was done in the r band following the standard MegaCam procedures. In the narrow-band filter, the photometric calibration was secured with the observation of the spectrophotometric standards Feige 34 and Hz44 (Massey et al. 1988). The observation of these standard stars gives consistent results within 2%. The images were taken in good seeing conditions (0.80 arcsec in r and 0.86 in Hα+[NII]).

2.2. Long-slit spectroscopy

The galaxy NGC 4569 was observed in 2001 with the Calar Alto 3.5 m telescope using the Twin spectrograph. Its was observed with the T05 and T06 gratings in the blue (4430 Å) and red (6562 Å) arm of the spectrograph with a dispersion of 36 Å/mm and a spatial sampling of 0.56 arcsec/pixel. Observations were obtained with a 30-min exposure using a 4 arcmin long slit of width 1.2 arcsec that was centered on the nucleus of the galaxy and oriented to a PA of 105°, as indicated in Fig. 6. Owing to the low signal to noise and sensitivity in the blue arm, we were not able to obtain reliable measurements for a detailed and satisfactory analysis of the data.

3. Data reduction

3.1. Narrow-band imaging

The data have been reduced using the Elixir-LSB package (Cuillandre et al., in prep.), a pipeline expressly developed to minimise the contribution of the scattered light component in MegaCam images. The efficiency of this observing strategy and data reduction procedures have been proven by the detection of very low surface-brightness features in the tidal tails associated with early-type galaxies in the MATLAS (Duc et al. 2011, 2015) and in the NGVS surveys (Ferrarese et al. 2012; Mihos et al. 2015).

The best ON- and OFF-band images were then combined to produce a Hα+[NII] (continuum-subtracted) frame (Fig. 2). The ON- and OFF-band frames are scaled using ad-hoc normalisation factors n, depending on the typical colour of the galaxy (Spector et al. 2012). The colour-dependent normalisation was determined using 15 stars of different colour in the observed field. The photometric calibration of the image obtained using the spectrophotometric standard stars was checked using a few galaxies in the field that had been observed during previous targeted narrow-band imaging observations or using nuclear spectroscopy from the SDSS (see Table 1). This comparison gives fairly consistent results (σ 0.25 dex).

Table 1. Hα+[NII] fluxes and equivalent widths of Virgo cluster galaxies with data in the literature.

Galaxy	This work log f(Hα+[NII]) erg s^{-1} cm^{-2}	This work Hα+[NII]E.W. Å	Literature log f(Hα+[NII]) erg s^{-1} cm^{-2}	Literature Hα+[NII]E.W. Å	Ref.
NGC 4569	–11.85 ± 0.02	3.1 ± 0.1	–12.02 ± 0.25	2 ± 1	1
			–11.24	–	2
			–11.62[b]	6 ± 2[b]	3
			–11.95 ± 0.07	–	4
			–11.83	–	5
IC 3583	–12.67 ± 0.02	12.1 ± 0.4	–12.17 ± 0.08	43.5 ± 12.2	6
NGC 4584	–13.07 ± 0.04	4.8 ± 0.3	–12.98 ± 0.19	7.5 ± 4.8	6
AGC 225847	–14.42 ± 0.08	17.3 ± 1.7	–14.30 ± 0.07	26.2 ± 4.5	7
VCC 1614[a]	–14.70 ± 0.01	8.4 ± 0.1	–14.75 ± 0.04	4.3 ± 0.5	8

Notes. [(a)] In the 3 arcsec SDSS aperture; [(b)] measured in a circular aperture of 7 arcmin diameter.

References. 1) Boselli & Gavazzi (2002); 2) Young et al. (1996); 3) Kennicutt & Kent (1983); 4) Sanchez-Gallego et al. (2012); 5) Koopmann et al. (2001); 6) Gavazzi et al. (2002); 7) Gavazzi et al. (2012); 8) Alam et al. (2015).

The pixel size in the raw images is of 0.187 arcsec/pixel. To increase the signal-to-noise we rebinned the images by a factor of three (0.561 arcsec/pixel) and later smoothed them using a median 5 × 5 pixel filter. At low-level counts the continuum-subtracted image also shows several low surface-brightness features. Some of them are clearly associated with the reflection of bright stars in the field, not fully removed by the Elixir-LSB data reduction procedure. Fortunately these are far from the target galaxy and only marginally affect the present analysis. The image also shows filamentary structures in the west of NGC 4569, which form a double tail that is clearly associated with the galaxy (see next section). The pixel 1σ rms of the resulting rebinned image is of 3.8×10^{-18} erg cm^{-2} s^{-1} arcsec^{-2}. Because the signal is extended on scales of a few arcseconds in the extended filaments that were detected in Hα+[NII], once smoothed, the image is sufficiently deep to detect features with a surface brightness of $\simeq10^{-18}$ erg cm^{-2} s^{-1} arcsec^{-2} (Fig. 2). The comparison of the continuum-subtracted image of the galaxy (Fig. 2) with the one obtained in a 30 min exposure with the 1.2 m OHP telescope (Fig. 3, Boselli & Gavazzi 2002) emphasises the exquisite quality of the present image. The total Hα+[NII] flux of the stellar disc measured within an elliptical aperture, arbitrary defined to minimise the contribution of IC 3583 (Fig. 4), is $\log f(\mathrm{H}\alpha + [\mathrm{NII}]) = -11.85 \pm 0.03$ erg s^{-1} cm^{-2}, which is consistent with previous estimates (see Table 1).

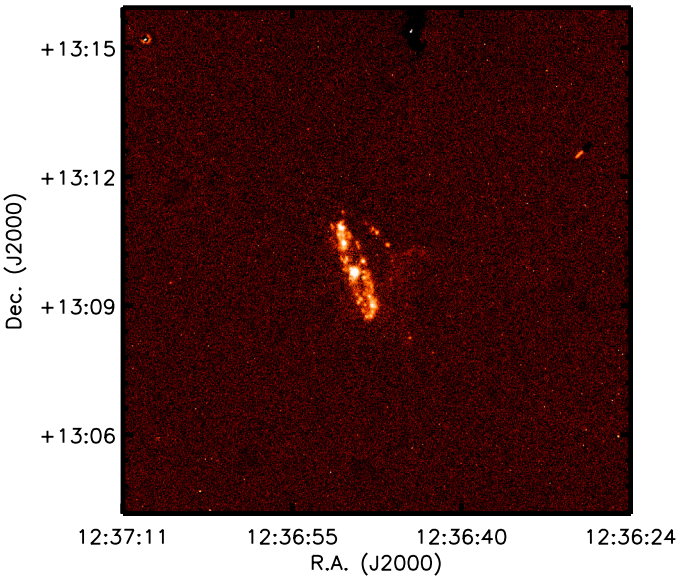

Fig. 3. Hα+[NII] image of NGC 4569 and IC 3583 obtained with a 30 min ON-band exposure at the 1.2 m telescope of the Observatoire de Haute Provence, from Boselli & Gavazzi (2002). The image covers the area shown as the white box in Fig. 2.

3.2. Long-slit spectroscopy

The reduction was performed using the *longslit* package in IRAF. We have used dome flats to create the spectroscopic flat field. Wavelength calibration has been performed using the Thorium-Argon lamp. The tilt of the dispersion axis with respect to the CCD rows has been corrected using a template that was created from observations of standard stars and the galaxy core at different positions along the slit.

From the sky-subtracted, continuum-subtracted, and wavelength-calibrated 2D spectrum (shown in Fig. 5) we have extracted 1D spectra in the regions that are given in Table 2 using median statistics. Variance spectra have been extracted in the same positions along the slit by assuming Poisson statistics on the un-sky-subtracted 2D spectrum. The spectral resolution ($R = \lambda/\Delta\lambda$) has been obtained by fitting 18 bright isolated sky lines in the spectrum in a position close to the galaxy nucleus. We then have fitted a third order polinomial to those points to obtain a model of R vs. wavelength which has been then used in the fitting procedure to correct the width of the lines for the instrumental resolution. The spectral resolution of the data is $R = 6290$ ($FWHM = 46$ km s^{-1} or 1.02 Å) at Hα.

We have fitted the emission line of the spectrum with the KUBEVIZ software[1] (Fossati et al. 2016). This code uses linesets, defined as groups of lines that are fitted simultaneously. Each lineset is described by a combination of 1D Gaussian functions where the relative velocity separation of the lines is kept fixed. In this work we have fitted two linesets, the first made up of Hα and [NII] $\lambda\lambda$6548, 6584 and the second made of [SII] $\lambda\lambda$6716, 6731. Furthermore, the flux ratio of the two [NII] lines has been kept constant in the fit to the ratios in Storey & Zeippen (2000). The continuum level has been evaluated during the fit procedure with an initial guess estimated in two symmetric windows

[1] http://www.mpe.mpg.de/~mfossati/kubeviz/

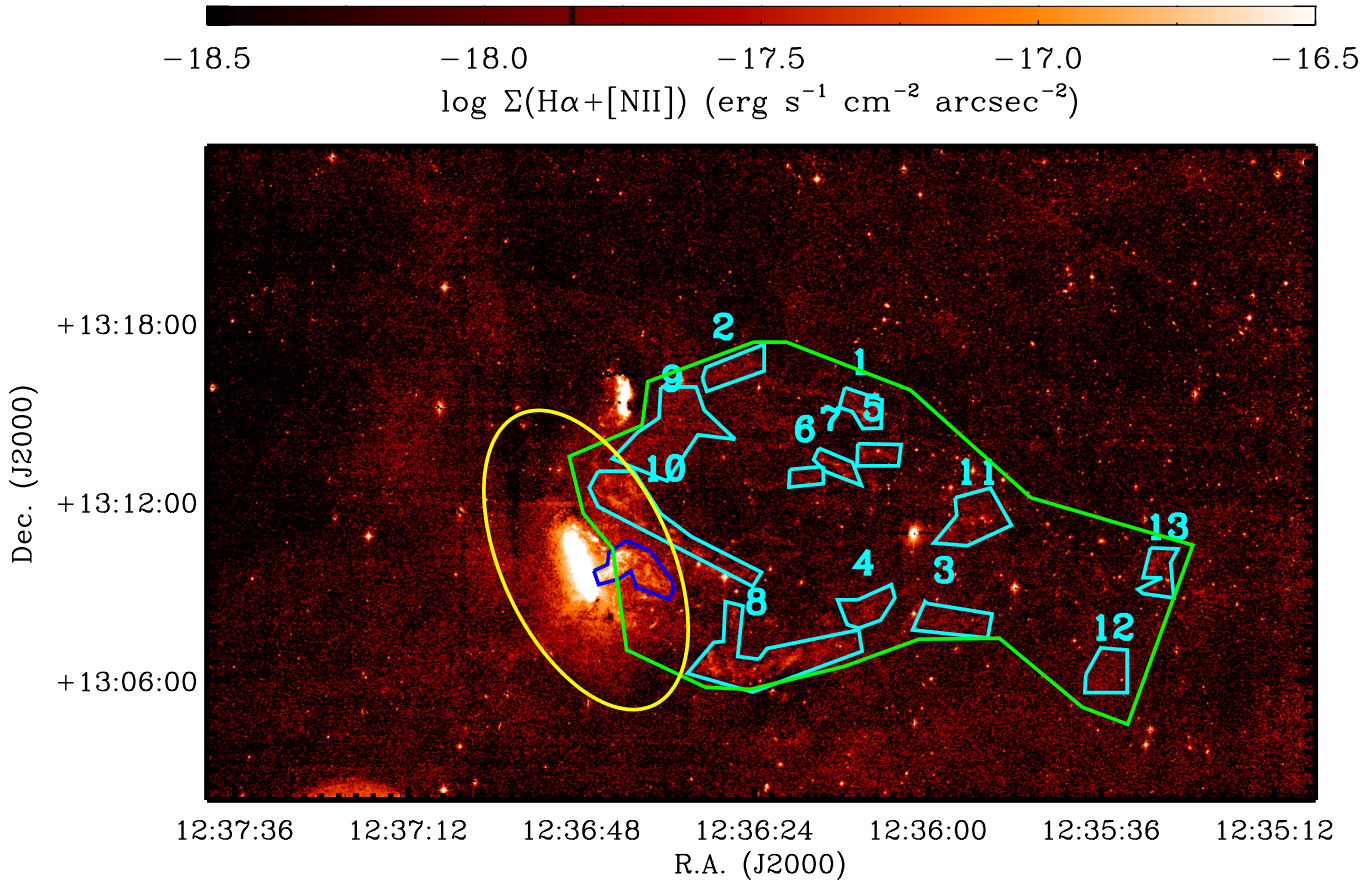

Fig. 4. CFHT MegaCam Hα+[NII] image of NGC 4569 and IC 3583 smoothed as in Fig. 1. The different low surface-brightness regions with Hα+[NII] emission are indicated with cyan polygons, and their surface brightness is listed in Table 3. The yellow elliptical aperture indicates the adopted extension of the galaxy within which its total Hα+[NII] flux has been measured (Table 1). The total emission within the tail has been measured within the large green polygon, while that of the nuclear outflow, within the blue polygon.

Table 2. Spectroscopic emission line measurements of the different regions shown in Figs. 6 and 5.

Region	Start	End	log(Hα/H$\alpha_{\rm nuc}$)	Δv	σ	[NII]λ6584/Hα	[SII]$\lambda\lambda$6716,6731/Hα	[SII]λ6716/[SII]λ6731
	$''$	$''$		(km s^{-1})	(km s^{-1})			
A	16	7	–1.9	82.6 ± 5.5	54.2 ± 6.1	1.39 ± 0.41	0.88 ± 0.28	1.48 ± 0.43
Nuc	3	–3	+0.0	3.2 ± 2.0	132.8 ± 2.1	1.29 ± 0.04	0.67 ± 0.02	1.10 ± 0.06
B	–9	–14	–1.7	24.4 ± 1.5	29.6 ± 1.8	0.69 ± 0.05	0.44 ± 0.04	1.40 ± 0.25
C	–21	–33	–2.7	10.6 ± 8.4	41.6 ± 8.8	2.15 ± 0.80	–	–
D	–49	–54	–1.8	60.0 ± 0.8	9.6 ± 1.7	0.37 ± 0.03	0.26 ± 0.02	1.74 ± 0.32
E	–67	–84	–2.2	128.4 ± 7.8	89.2 ± 8.2	0.85 ± 0.12	0.48 ± 0.08	1.20 ± 0.30
F	–84	–89	–2.4	84.1 ± 11.4	73.8 ± 12.8	0.79 ± 0.21	–	–
G	–89	–96	–2.1	48.8 ± 4.8	79.1 ± 4.9	1.06 ± 0.11	0.77 ± 0.09	1.51 ± 0.32
H	–96	–104	–2.4	–13.9 ± 8.6	90.6 ± 9.5	1.30 ± 0.22	–	–

Notes. Region Nuc corresponds to the nucleus of NGC 4569. Start and End denote the position in arcseconds with respect to the photometric centre where the 1D extraction is performed. log(Hα/H$\alpha_{\rm nuc}$) is the brightness of the Hα line in a given region normalised to that of the nucleus. Δ_V is given with respect to the systemic velocity of NGC 4569 (−221 km s^{-1}).

around each lineset. During the fit, KUBEVIZ takes into account the noise from the variance spectra, thus it optimally suppresses the sky line residuals which bracket the Hα line at the redshift of NGC 4569. However, the adopted variance underestimates the real error, most notably because it does not account for correlated noise that is introduced in the reduction procedure and extraction of 1D spectra. We have therefore renormalised the final errors on the line fluxes and kinematical parameters, assuming a $\chi^2 = 1$ per degree of freedom. The resulting emission line measurements are given in Table 2. We have verified that the kinematical parameters are consistent within the uncertainties if we compare the two linesets (Hα+[NII] and [SII]). Nonetheless, the values listed in Table 2 have been obtained from the first lineset because the uncertainties are smaller as a result of the brighter lines. Diagnostic line ratios are also given whenever the signal-to-noise of all the lines involved in the ratio is greater than three.

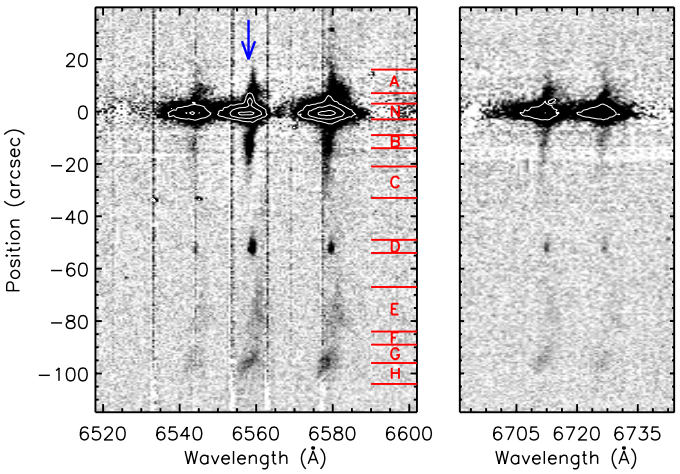

Fig. 5. 2D continuum subtracted spectrum of NGC 4569 zoomed on the Hα and [NII] lines (*left*) and on the [SII] doublet (*right*), as obtained at Calar Alto with a slit of width 1.2 arcsec positioned along the minor axis on the spur of ionized gas as indicated in Fig. 6. The red labels shown in the left panel correspond to those shown in Fig. 6 and indicate the range of pixels used to extract 1D spectra to derive the physical parameters given in Table 2. The blue vertical arrow shows the mean recessional velocity of the galaxy (−221 km s^{-1}) derived from HI data.

4. Physical parameters

4.1. Narrow-band imaging

The deep Hα+[NII] image of NGC 4569 shows several filamentary features extending from the disc of the galaxy to ∼80 kpc projected distance to the west. These filaments are dominated by two main features, as often observed in cluster galaxies with extended tails of ionized gas (Sun et al. 2007, 2010; Yagi et al. 2010). The Hα+[NII] fluxes of NGC 4569 and of its associated low surface-brightness extended features (Table 3), as well as those of the other galaxies in the frame (Table 1) are determined by measuring the counts in the ON- and OFF-band frames (after removing the contribution of unwanted foreground stars in the field). The flux of all these targets has been extracted using the QPHOT IRAF task whenever possible. For sources with asymmetric distributions or with evident nearby companions, which might significantly contaminate the flux, we used the FUNTOOLS analysis package on DS9. For these sources, we manually defined elliptical apertures that were adjusted to fit the full light profile of each target galaxy and we also selected uncontaminated regions to determine the background of the sky. Using polygons, we identified in the image, which had been smoothed with a median filter of 5 × 5 pixels, a number of low surface-brightness features, as labeled in Fig. 4. Their flux was extracted using FUNTOOLS, while the local sky background was estimated in adjacent polygons. We also extracted the total flux of all the extended filaments using a large polygon that covers the western part of the galaxy, with its associated sky background measured in several circular apertures that were located in uncontaminated regions around it. The uncertainty of these measurements was determined using the prescription given in Boselli et al. (2003), which is optimised for extended sources where the uncertainty is dominated by large scale fluctuations of the sky background (see also Ciesla et al. 2012). The properties of these regions are listed in Table 3.

The Hα luminosity of the different galaxies and of the extended features can be determined once the observed fluxes have been corrected for [NII] contamination. This is relatively easy

Table 3. Hα+[NII] flux and surface brightness of the low surface brightness features.

Region	log f(Hα+[NII]) erg s^{-1} cm^{-2}	Σ(Hα + [NII]) 10^{-19} erg s^{-1} cm^{-2} arcsec^{-2}	Area arcsec^2
Tail	−12.52 ± 0.36	5.2 ± 4.4	573 619
Outflow	−13.07 ± 0.02	88.2 ± 4.4	9625
1	−14.19 ± 0.13	14.4 ± 4.4	4537
2	−14.19 ± 0.18	10.5 ± 4.4	6185
3	−14.14 ± 0.20	9.3 ± 4.4	7743
4	−14.22 ± 0.18	10.7 ± 4.4	5628
5	−14.35 ± 0.16	11.8 ± 4.4	3773
6	−14.59 ± 0.18	10.7 ± 4.4	2404
7	−14.40 ± 0.15	12.4 ± 4.4	3251
8	−13.41 ± 0.12	16.2 ± 4.4	24 350
9	−13.61 ± 0.16	11.9 ± 4.4	20 417
10	−13.39 ± 0.09	21.2 ± 4.4	19 146
11	−13.90 ± 0.15	12.3 ± 4.4	10 220
12	−14.12 ± 0.17	11.4 ± 4.4	6667
13	−14.26 ± 0.17	11.0 ± 4.4	5038

for the emission over the discs of the two galaxies NGC 4569 and IC 3583, an irregular galaxy at a projected distance of ∼6 arcmin, for which integrated spectroscopy is available from Gavazzi et al. (2004) and Boselli et al. (2013)[2]. The physical conditions of the stripped interstellar medium might be significantly different over the disc of the galaxy, thus this ratio might change significantly. In particular, the radiation of the hot gas of the intracluster medium is expected to increase the [NII]/Hα ratio. Recent spectroscopic observations done with the Multi Unit Spectroscopic Explorer (MUSE) of ESO 137-001, a galaxy in the Norma cluster that is undergoing a stripping process similar to the one occurring in NGC 4569, suggest that the [NII]/Hα ratio in the tail is not typical of a photoionization region ([NII]/Hα ≃ 0.3), but is slightly higher, which is probably because the gas is partly excited by shocks or by heat conduction ([NII]/Hα ≃ 0.5, Fossati et al. 2016). Similar results have been derived from the spectroscopic observations of the tails of other cluster galaxies (Yagi et al. 2007; Yoshida et al. 2012; Merluzzi et al. 2013). We thus assume [NII]/Hα = 0.5 in the tails.

An estimate of the density of the ionized gas can be derived using the relation

$$L(\mathrm{H}\alpha) = n_\mathrm{e} n_\mathrm{p} \alpha^{\mathrm{eff}}_{\mathrm{H}\alpha} V f h \nu_{\mathrm{H}\alpha} \quad (1)$$

(Osterbrock & Ferland 2006), where n_e and n_p are the number density of electrons and protons, $\alpha^{\mathrm{eff}}_{\mathrm{H}\alpha}$ is the Hα effective recombination coefficient, V is the volume of the emitting region, f the filling factor, h the Planck's constant, and $\nu_{\mathrm{H}\alpha}$ the frequency of the Hα transition. The two variables V and f can only be crudely estimated from observations or from simulations.

The stripped material is assumed to be distributed in a cylinder of diameter (≃50 kpc) and of height comparable to the extension of the observed tail of ionized gas. In the case of NGC 4569, the tail extends up to ≃ 80 kpc on the plane of the sky. Since the galaxy is blue-shifted (vel = −221 km s^{-1}), we assume that it is crossing the cluster from the backside. It is conceivable that the observed tail of ionized gas is just a projection on the plane of the sky, thus that 80 kpc is a lower limit to the real height of the cylinder. The comparison of multifrequency observations of the galaxy with tuned models of gas stripping suggest that the galaxy underwent the peak of the stripping process ≃100 Myr ago

[2] We use the updated value of [NII]/Hα = 0.97 for NGC 4569 given in Boselli et al. (2015) for this purpose.

(Boselli et al. 2006). At a radial velocity of ≃1100 km s^{-1} with respect to the cluster centre[3], the galaxy would have traveled ∼120 kpc along the line of sight. Summing these values quadratically, we expect that the physical extension of the stripped gas is ∼145 kpc, corresponding to ∼5.5 times the optical radius of the galaxy.

The filling factor f is another unconstrained parameter. In all galaxies where tails have been observed, the ionized gas has a structured distribution, with high density clumps of condensed material that is often associated with star-forming regions, otherwise extended in filamentary structures (Yagi et al. 2007, 2010, 2013). Similar structures are also present in hydrodynamic simulations (e.g. Tonnesen & Bryan 2010). In particular, the filamentary structures with double tails are reproduced in simulations whenever magnetic fields are taken into account (Ruszkowski et al. 2014; Tonnesen & Stone 2014). It is thus most likely that $f < 1$, but its exact value is highly uncertain. Consistent with previous works, which generally take $0.05 < f < 0.1$, we assume $f = 0.1$.

If we assume that the gas is fully ionized, so that $n_e = n_p$, and $\alpha^{\rm eff}_{\rm H\alpha} = 1.17 \times 10^{-13}$ cm^3 s^{-1} (Osterbrock & Ferland 2006) the density of the gas can be derived from Eq. (1):

$$n_e = \sqrt{\frac{L(\mathrm{H}\alpha)}{\alpha^{\rm eff}_{\rm H\alpha} V f h \nu_{\rm H\alpha}}}. \quad (2)$$

Under these assumptions, the mean density of the ionized gas is $n_e \simeq 5 \times 10^{-3}$ cm^{-3}, and the total mass of the ionized gas is $M_{\rm tail}(\mathrm{H}\alpha) \simeq 3.2 \times 10^9\ M_\odot$. Given the high degree of uncertainty in the geometry of the gas, this is a very rough estimate. We can also calculate the typical density of the gas within the different filaments labelled in Fig. 4. Assuming a cylindrical geometry, the typical density within the different filaments ranges between 2 and 4×10^{-2} cm^{-3}, while the total mass in the 13 identified regions is $\simeq 3.1 \times 10^8\ M_\odot$[4].

4.2. Long-slit spectroscopy

4.2.1. Kinematics

The spectral resolution of the Calar Alto observations is sufficient to study the kinematics of the ionized gas along the slit (see Table 2). The 2D-spectrum of the galaxy (Fig. 5) shows an offset in velocity in the SE (region A, extending up to ≃20 arcsec) and NW (region B, up to ≃30 arcsec). This offset, which is also observed in the Hα Fabry-Perot data of Chemin et al. (2006), is due to the rotation of the galaxy. This region corresponds to the Hα main body of the galaxy in Fig. 6. The nuclear spectrum also shows a large velocity dispersion (132 km s^{-1}) that is due to the turbulence in the gas that was probably induced by a nuclear activity (Ho et al. 1997). A high surface brightness region is detected at ∼50 arcsec from the nucleus in the NW direction (region D). This region, which is located in the projection of the extended NW spiral arm, is also present in the Fabry-Perot data. The velocity dispersion of this region is low (≃10 km s^{-1}) and is typical of an HII region. Further out, emission is detected along the filaments of ionized gas at high velocity (up to ≃130 km s^{-1} in region E) with respect to the nucleus. The kinematic of the gas, as shown in Fig. 5, is totally disconnected from the rotation of the disc. Further out (Regions F, G), the recessional velocity decreases smoothly, then rapidly in Region H, where it reaches negative values. The velocity dispersion in these outer and diffuse regions is relatively high (70−90 km s^{-1}), indicative of the presence of turbulent motions.

4.3. Line ratios

We can also estimate how the [NII], Hα, and [SII] line ratios change along the slit in the different positions listed in Table 2. The [NII]/Hα line ratio in the nucleus is 1.29 ± 0.04, while [SII]/Hα = 0.67 ± 0.02. These values are typical of LINER galaxies (e.g. Ho et al. 1997). The values of region D ([NII]/Hα = 0.37 ± 0.03; [SII]/Hα = 0.26 ± 0.02) are typical of HII regions, confirming that this high surface brightness spot is a star-forming region that is associated with the western spiral arm. The values of [NII]/Hα and [SII]/Hα measured in all other regions, on the contrary, are in the range $0.7 \lesssim$ [NII]/Hα $\lesssim 1.4$ and $0.4 \lesssim$ [SII]/Hα $\lesssim 0.9$. Although uncertain, these values are too high to be produced only by stellar photoionization, and so require the contribution of a hard radiation field like the one produced by a nearby nucleus or by slow shocks (Tüllmann et al. 2000; Allen et al. 2008; Rich et al. 2011). In the spur of ionized gas the [SII]λ6716/[SII]λ6731 line ratio is ≃1.4, which suggests that the electron density of gas is low ($n_e \lesssim 10$ cm^{-3}). The exact value is poorly constrained given the large uncertainty on the [SII] ratio and the saturation in the intensity ratio vs. electron density relation (Osterbrock & Ferland 2006).

5. Comparison with multifrequency data

High-quality multifrequency data covering the whole electromagnetic spectrum, from X-ray to radio, of NGC 4569 are available in the literature. These data are crucial for a comparison with the Hα data obtained in this work to identify the perturbing mechanism that affects the galaxy. Excellent quality *ugiz* imaging data of NGC 4569 have been obtained as part of the NGVS survey using MegaCam at the CFHT (Ferrarese et al. 2012). The pseudo-colour optical image of the galaxy is shown in Fig. 7 and 8. The optical image does not show any diffuse stellar emission down to a surface brightness limit of ≃29 μ_g mag arcsec^{-2} (AB system) that is associated with the stripped ionized gas, which is located in the west of the galaxy. The lack of low surface-brightness stellar features, which are generally formed during gravitational interactions with nearby companions, suggests that the gaseous component is removed from the galaxy through the interaction with the hot and dense intracluster medium. The comparison of the Hα frame with the optical NGVS (Fig. 7) and the far (FUV) and near-ultraviolet (NUV) (Figs. 9 and 11) images of the galaxy that were obtained as part of the the GUViCS survey of the cluster (Boselli et al. 2011) also indicates that the ionized gas is only diffuse and does not have any kind of clumpy structure, which suggests the presence of extraplanar HII regions. The smallest resolved features in the Hα+[NII] image have a filametary structure of thickness larger than 200 pc. We note that the NUV image of the galaxy and its surrounding regions was obtained with a very long exposure (16 993 s) and it is thus very sensitive to extraplanar star-forming regions, such as those observed around M49 (Arrigoni-Battaia et al. 2012) or VCC 1217 (Hester et al. 2010; Fumagalli et al. 2011; Kenney et al. 2014). The Hα+[NII] surface brightness of the extraplanar HII region which are associated with these two galaxies is $\sim 2 \times 10^{-17}$ erg cm^{-2} s^{-1} arcsec^{-2}, thus well above the

[3] The mean velocity of Cluster A, the Virgo substructure to which NGC 4569 belongs, is *vel* = 955 km s^{-1} (Boselli et al. 2014a).

[4] This value should be taken as a lower limit to the total mass of the ionized gas given that the 13 regions indicated in Fig. 4 do not include all the low surface-brightness filaments associated with the galaxy.

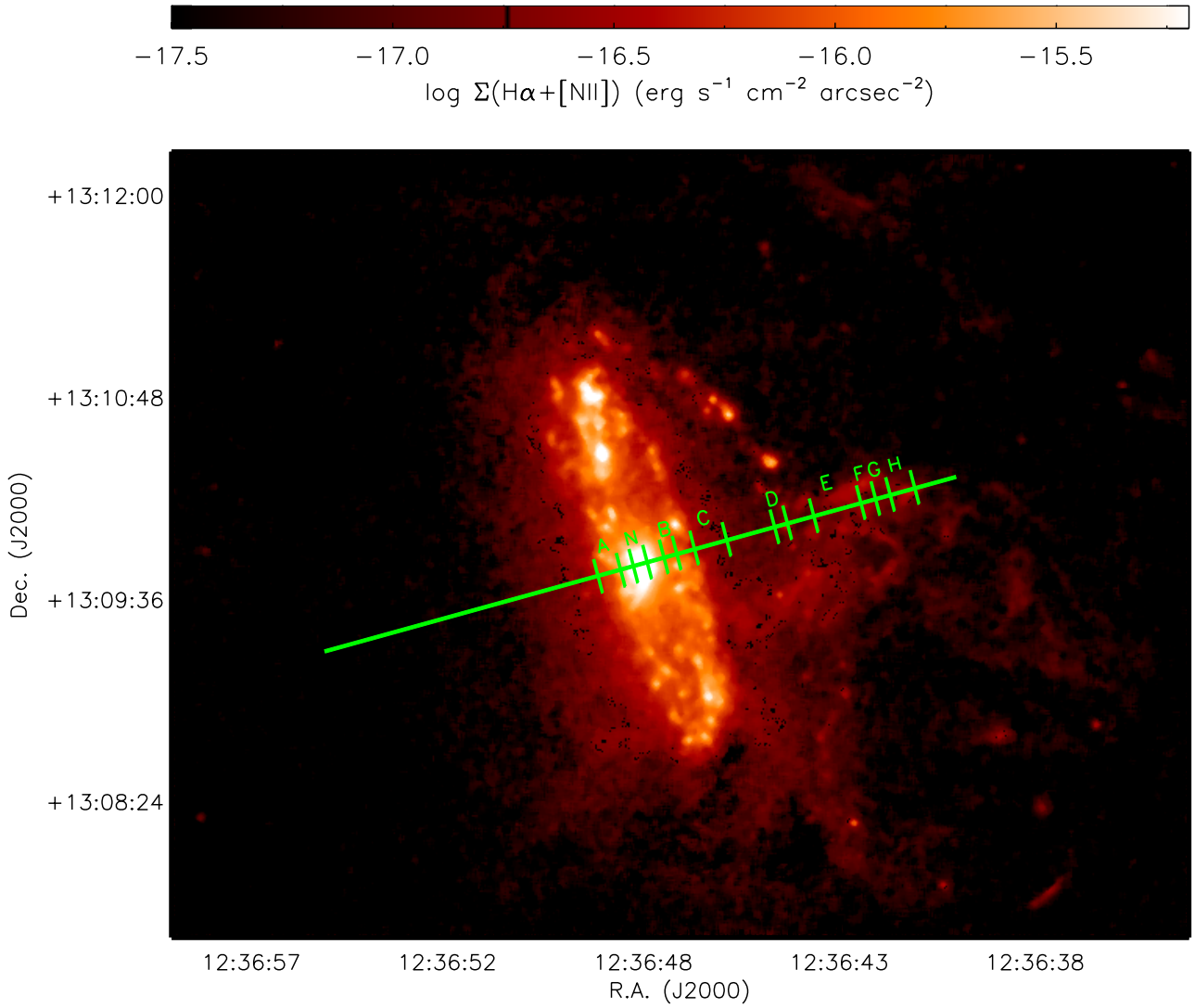

Fig. 6. CFHT MegaCam Hα+[NII] image of the star-forming disc and of the nuclear outflow of NGC 4569. The green line indicates the position of the long slit in the Calar Alto spectroscopic observations. The different letters indicate the various regions used to extract 1D spectra and derive the physical parameters listed in Table 2. They corresponds to those indicated in Fig. 5.

detection limit of our image. The limiting sensitivity in the NUV image is of ≃29 AB mag arcsec^{-2}, thus deep enough for detecting low surface-brightness features, such as those observed in the tidal tails of NGC 4438 (Boselli et al. 2005).

The distribution of the atomic gas was mapped using the VLA in C short configuration by Chung et al. (2009). The HI image, which has an angular resolution of 15−16 arcsec and a column density sensitivity of $3-5\times10^{19}$ cm^{-2} (3σ per channel), shows that the HI gas is located within the stellar disc of the galaxy and has a truncated radial distribution that is typical of HI-deficient cluster galaxies (Cayatte et al. 1994; Chung et al. 2009). This is also the case for the distribution of the molecular gas (Helfer et al. 2003) and of the hot and cold dust components as derived from WISE, *Spitzer*, and *Herschel*[5] images (Boselli et al. 2006; Cortese et al. 2014; Ciesla et al. 2012; Fig. 10). The atomic gas and the dust component are not detected along the tails of ionized gas.

Rosat, *XMM-Newton*, *Chandra* X-ray, and VLA 1.4, 4.86 GHz radio continuum images of NGC 4569 show extended features that are perpendicular to the stellar disc of the galaxy (Tschoeke et al. 2001; Chyzy et al. 2006; Grier et al. 2011; Wezgowiec et al. 2011, 2012). The extension of the hot gas traced by the 0.2−1 keV *XMM-Newton* X-ray image, however, is smaller than that of the ionized gas (Figs. 10 and 11). The 20 cm radio continuum emission, however, is limited to the inner 22 kpc and does not morphologically match the ionized gas.

6. Discussion

6.1. The galaxy

NGC 4569 shows a truncated star-forming disc with respect to the distribution of the old stellar populations (Boselli et al. 2006), with a prominent spiral arm starting from the north of the galaxy and extending in a westerly direction. The excellent quality of the CFHT image shows resolved HII regions along the disc and the western spiral arm. A concentration of HII regions is present on the north-east and south-west star-forming disc, suggesting a grand design spiral pattern drawn by two major spiral

[5] NGC 4569 has been observed during the *Herschel* Reference Survey (Boselli et al. 2010). Most of these multifrequency data are available on a dedicated database: http://hedam.lam.fr/HRS/

Fig. 7. Pseudo-colour image of NGC 4569 and IC 3583 obtained when combing the CFHT MegaCam NGVS optical *g* (blue) and *i* (green) images with the Hα+[NII] narrow-band image (red). North is up, east left.

arms. Independent tracers of star formation, including the Hα flux derived in this work, can be converted under some assumptions into star formation rates (e.g. Kennicutt 1998; Boselli et al. 2009). The star formation rate measured over the whole disc of NGC 4569 is $SFR \simeq 2\ M_{\odot}\,\mathrm{yr}^{-1}$, assuming a Salpeter IMF (Boselli et al. 2015).

The wavelength-dependent truncation of the stellar disc and of the gas (atomic and molecular), and dust components observed in NGC 4569 has been explained as being due to a recent ($\simeq$100 Myr) ram pressure stripping event that was capable of radially removing the gaseous component and gradually quenching the activity of star formation of the galaxy in the outer regions (Boselli et al. 2006). A similar timescale ($\simeq$300 Myr) was derived from the study of the kinematic properties of the atomic gas (Vollmer et al. 2004) and from the analysis of 2D optical spectra (Crowl & Kenney 2008). Thus, the physical and kinematic properties of the main body of NGC 4569 consistently indicate that the galaxy underwent a recent ram pressure stripping event. We want to see whether this evolutionary picture can also explain the presence of the low surface-brightness features detected in the Hα+[NII] narrow-band image described in the previous section.

6.2. The nuclear outflow

The deep MegaCam Hα+[NII] image shows a diffuse and extended halo of ionized gas around the galaxy. It also shows a prominent plume in the western side that is perpendicular to the disc. This plume is located south of the minor axis in the region between the star-forming disc and the prominent western spiral arm, and along the minor axis outside it (see Fig. 4). Its total extension is $\simeq$100 arcsec (8 kpc), and its total flux is $\log f(\mathrm{H}\alpha + [\mathrm{NII}]) = -13.07\ \mathrm{erg\,s^{-1}\,cm^{-2}}$ (see Table 3). The presence of a prominent dust lane on the western side of the galaxy (Fig. 8), hidden by the bulge on the eastern side, suggests that the western side is the near side. The spur of gas observed on the western side has a higher recessional velocity with respect to the nucleus of the galaxy and is thus an outflow. The nuclear outflow is probably powered by a nuclear starburst (Barth et al. 1998; Maoz et al. 1998; Barth & Shields 2000; Tschoeke et al. 2001; Chyzy et al. 2006). The spectral synthesis analysis of the nuclear HST spectra carried out by Barth & Shields (2000), who classified it as a typical LINER/HII transition nucleus, date the nuclear ($\lesssim$30 pc) starburst as ~3−6 Myr (Barth & Shields 2000; Gabel & Bruhweiler 2002). The presence of A-type supergiants in the inner ~300 pc suggests that a second starburst occurred more than 15 Myr ago (Keel 1996). A contribution from an AGN cannot be fully excluded, given the presence of a compact source in the soft *Chandra* X-ray image of NGC 4569 (Grier et al. 2011). A dominant AGN activity, however, is ruled out by the lack of a point-like nuclear source in the radio continuum (Hummel et al. 1987; Neff & Hutchings 1992) and in the ROSAT X-ray hard-band image of the galaxy (Tschoeke et al. 2001).

If we assume that the gas is mainly photoionized, we can use Eq. (2) to estimate the total density and mass of the ionized gas in the outflow. Assuming that the gas in the outflow is in

Fig. 8. Pseudo-colour image of NGC 4569 and IC 3583 obtained using the CFHT MegaCam NGVS (Ferrarese et al. 2012) optical *u* (blue), *g* (green), and *i* (red) images. North is up, east left.

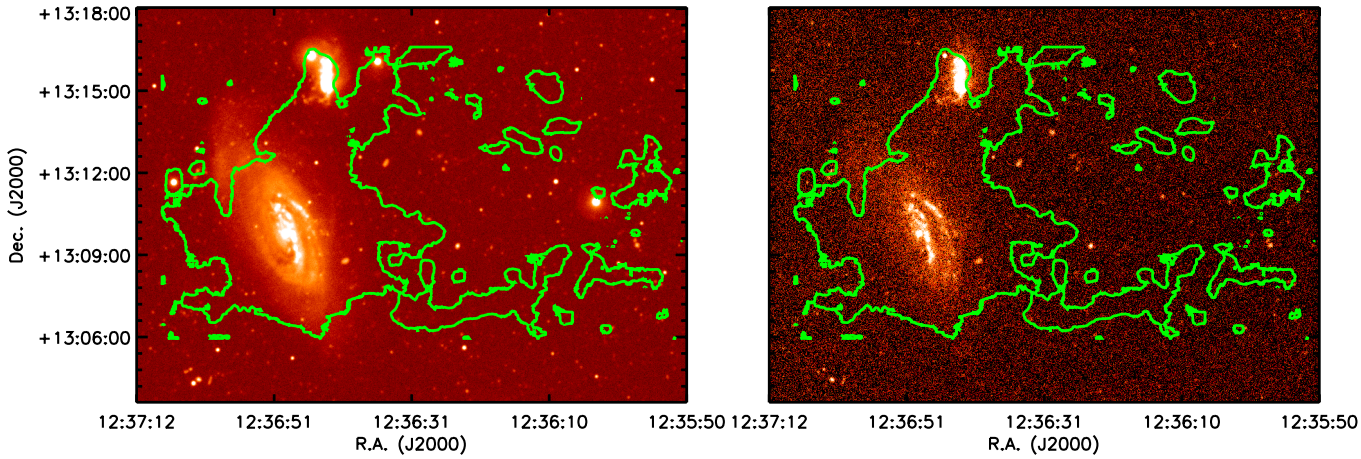

Fig. 9. GALEX NUV (*left*) and FUV (*right*) images of NGC 4569 with contour levels showing the Hα+[NII] surface-brightness level of 10^{-18} erg s^{-1} cm^{-2} arcsec^{-2}.

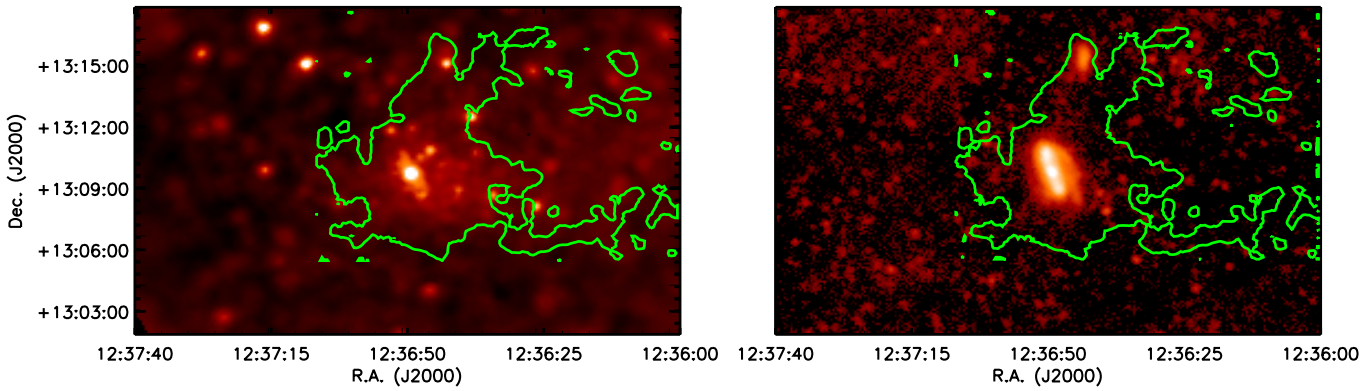

Fig. 10. The 0.4−1.3 keV background-subtracted and exposure-corrected X-ray (*left*) XMM image and the far-infrared 250 μm (*right*; Ciesla et al. 2012) images of NGC 4569 with contour levels showing the Hα+[NII] surface-brightness level of 10^{-18} erg s^{-1} cm^{-2} arcsec^{-2}.

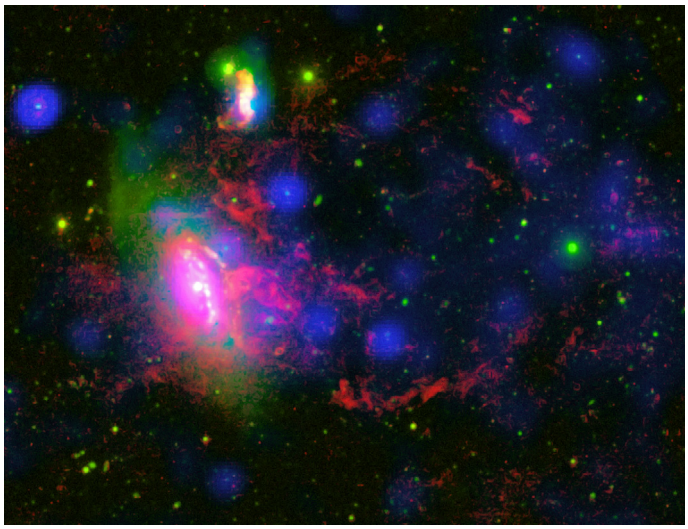

Fig. 11. Pseudo-colour image of NGC 4569 and IC 3583 obtained by combining XMM 0.4−1.3 keV X-rays (blue), GALEX NUV (green), and CFHT MegaCam Hα+[NII] (red) images. North is up, east left.

Table 4. Parameters of NGC 4569 and IC 3583.

Variable	NGC 4569	Ref.	IC 3583	Ref.
Morph. type	SAB(rs)ab;LINER;Sy	1	IBm	1
D (Mpc)	$\gtrsim$17	2	9.52 ± 0.95	2
r_{25}	22.8 kpc	3	6.9	4
vel	–221 km s^{-1}	5	1120	5
$r/R_{\rm vir}$	0.32	TW	0.32	TW
$M_{\rm star}$ ($M_\odot$)	3.0×10^{10}	6	6.3×10^{8}	6
$M_{\rm dyn}$ ($M_\odot$)	1.2×10^{11}	7	–	
M(HI) ($M_\odot$)	7.6×10^{8}	5	4.7×10^{8}	5
$M(H_2)^a$ ($M_\odot$)	4.9×10^{9}	8	$<2.8 \times 10^{7}$	9
M(X-rays) ($M_\odot$)	$\lesssim 2 \times 10^{8}$	10	–	–
$M_{\rm tail}$(Hα) ($M_\odot$)	3.2×10^{9}	TW	–	–
$M_{\rm out}$(Hα) ($M_\odot$)	3.4×10^{7}	TW	–	–

Notes. $^{(a)}$ Derived using a constant $X_{\rm CO} = 2.3 \times 10^{20}$ cm^{-2}/(K km s^{-1}) conversion factor (Boselli et al. 2002).

References. 1) NED; 2) Karachentsev et al. (2014); 3) g-band isophotal radius, from Cortese et al. (2012b); 4) GOLDMine (Gavazzi et al. 2003); 5) Haynes et al. (2011); 6) derived from i-band luminosities using the $g - i$ colour-dependent stellar mass-to-light ratio relation from Zibetti et al. (2009) and assuming a Chabrier (2003) initial mass function; 7) Haan et al. (2008); 8) Boselli et al. (2014b); 9) Boselli et al. (2002); 10) Wezgowiec et al. (2011).

a cylinder of 60 arcsec (5 kpc) diameter and 96 arcsec (8 kpc) projected length, [NII]/H$\alpha \simeq 1$, and a filling factor $f = 0.1$, the density of the ionized gas is $n_{\rm e} \simeq 9.7 \times 10^{-2}$ cm^{-3} and its total mass $M_{\rm out}$(Hα) $\simeq 3.4 \times 10^7$ $M_\odot$ (see Table 4). This density is consistent with the mean electron density $n_{\rm e} \lesssim 10$ cm^{-3} , which is derived by the poorly constraining [SII]λ6716/[SII]λ6731 line ratio of the outflow ($\simeq$1.4). At this density, the recombination time is $t_{\rm rec} \simeq 1$ Myr, which is shorter than the age of the nuclear starburst. For an outflow velocity of $\simeq$130 km s^{-1}, the ejected gas should only have travelled a distance of $\simeq$0.65 kpc in 5 Myr, and $\gtrsim$2 kpc if powered by an older (>15 Myr) starburst episode that would have been necessary to explain the presence of A-type supergiants in the inner 300 pc (Keel 1996). These distances are too small compared to the typical extension of the spur of ionized gas ($\simeq$8 kpc). It is thus conceivable that the gas in the outflow ionized by mechanisms other than photoionization from the central starburst. These can be identified as the nuclear activity or the shock that was induced by the turbulence in the outflow.

We can also make a rough estimate of the total (potential and kinetic) energy of the outflow. Considering the outflow as a cylinder of physical length H and radius r, its potential energy can be derived using the relation

$$\begin{aligned} {\rm d}\Phi_{\rm out} &= G\frac{M_{\rm N4569+out}}{h}{\rm d}M_{\rm out} \\ &= G(\rho_{\rm N4569} + \rho_{\rm out})(\pi r^2)^2 H \rho_{\rm out}\frac{{\rm d}h}{h}, \end{aligned} \quad (3)$$

where $\rho_{\rm N4569}$ and $\rho_{\rm out}$ are the mean mass density of the galaxy and of the gas in the outflow. The density of the galaxy can be inferred from its rotational velocity $vel_{\rm N4569}(r) \simeq 250$ km s^{-1} at a radius $r = 8$ kpc (Rubin et al. 1989) using the virial theorem ($\rho_{\rm N4569} \simeq 4.9 \times 10^{-24}$ g cm^{-3}), while that of the outflow is the one previously derived from the Hα luminosity ($\rho_{\rm out} \simeq 1.4 \times 10^{-25}$ g cm^{-3}). The potential energy of the outflow is thus $\Phi_{\rm out} \simeq 9 \times 10^{55}$ ergs. The kinetic energy of the outflow is:

$$E_{\rm kin,out} = \frac{vel_{\rm out}^2}{2} M_{\rm out}, \quad (4)$$

where $M_{\rm out}$ is the mass of the outflow ($M_{\rm out} = 3.4 \times 10^7$ $M_\odot$, see Table 4) and $vel_{\rm out}$ its velocity, corrected for the orientation of the

galaxy on the plane of the sky ($vel_{\rm out} \simeq 260$ km s^{-1}, see Table 2). The kinetic energy of the outflow is $E_{\rm kin,out} \simeq 2.4 \times 10^{55}$ ergs and the total energy is $E_{\rm tot,out} \simeq 1.1 \times 10^{56}$ ergs. This energy would require 1.1×10^5 supernovae of energy 10^{51} ergs, or a larger number if we assume a more realistic 1−10% energy transfer efficiency. To provide this number of supernovae, the nuclear star cluster would have to have a mass $\gtrsim 2.4 \times 10^7$ $M_\odot$ and a star formation rate of $\gtrsim 24$ $M_\odot$ yr^{-1}. The required mass and star formation activity of the nuclear starburst are a few order of magnitudes higher than those observed in the galaxy (Keel 1996; Barth & Shield 2000, Boselli et al. 2015). We caution, however, that ram pressure can produce low-density superbubble holes in the inner disc and thus supply extra energy to the outflow through Kelvin-Helmholtz instabilities (Roediger & Hensler 2005) and viscous stripping (Roediger & Bruggen 2008). Despite this possible increase of the efficiency in the energy transfer to the outflow as a result of ram pressure, this simple calculation suggests a probable suply of energy by an AGN.

The striking velocity difference between the adjacent regions G and H (∼60 km s^{-1}) can be explained by the fact that, while Region G is associated with the nuclear outflow, in Region H the ionized gas may have been stripped from the disc of the galaxy and is only located in projection close to the outer extension of the outflow. Indeed, a closer inspection of Fig. 6 shows that Region H is a few arcsec below the projection of the nuclear outflow.

6.3. The diffuse gas

The rough estimate of the total mass of the ionized gas which we derived from Hα emission in the diffuse tail in Sect. 4, is $M_{\rm tail}$(Hα) $\simeq 3.2 \times 10^9$ $M_\odot$ (Table 4). This mass can be compared to the total dynamical mass of the galaxy (1.2×10^{11} $M_\odot$, Haan et al. 2008) and to the mass of gas in the other gaseous phases. This galaxy has a total mass of molecular hydrogen of $M(H_2) = 4.9 \times 10^9$ or 2.2×10^9 $M_\odot$, depending on whether the molecular gas mass is derived from CO observations using a constant or variable CO-to-H_2 conversion factor (Boselli et al. 2014b). The total HI mass of NGC 4569 is 7.6×10^8 $M_\odot$ (Haynes et al. 2011) and is about a factor of ten smaller than that of isolated galaxies of similar type and luminosity, as indicated by its large HI-deficiency parameter ($HI - def$[6] = 1.05, Boselli et al. 2014b). This suggests that NGC 4569 has lost $\simeq 7.7 \times 10^9$ $M_\odot$ of HI. A more accurate estimate of the total mass of gas lost by the galaxy during its interaction with the cluster environment can be derived from a multizone chemo-spectrophotometric model of galaxy evolution (Boselli et al. 2006). The truncated gaseous and stellar profiles of NGC 4569 can be reproduced if the galaxy lost $\simeq 1.9 \times 10^{10}$ $M_\odot$ of gas during a ram pressure stripping event that started ∼100 Myr ago. This mass is slightly larger than the very rough estimate of the ionized gas mass derived from Hα and suggests that a large fraction of the atomic gas, once stripped, is ionized within the tail. The deep VLA 21 cm observations of the VIVA survey detect HI gas only within the stellar disc of NGC 4569 (Chung et al. 2009). A comparison of the HI and Hα+[NII] frames of the galaxy does not show the presence of any HI extraplanar feature that is associated with the tails of ionized gas down to a column density limit of $3-5 \times 10^{19}$ cm^{-2} for a 10 km s^{-1} spectral resolution (Chung et al. 2009). If all the stripped HI gas ($\simeq 1.9 \times 10^{10}$ $M_\odot$) was still in its neutral phase and was distributed within the same tail defined by the Hα+[NII] emission, its column density should be Σ(HI) $\simeq 0.4$ $M_\odot$ pc^{-2} ($\sim 5 \times 10^{19}$ at cm^{-2}), close to the detection limit of the VLA images. This, however, is probably a lower limit since we expect that the gas, as indicated by the observations of the ionized phase or by the simulation of the HI phase (Tonnesen & Bryan 2010) should have a clumpy distribution with peaks in column density well above this limit. The MUSE observations of ESO 137-001 show that the kinematical properties of the stripped gas do not significantly change with respect to that of the parent galaxy (Fumagalli et al. 2014). We thus expect that the stripped gas is distributed in the same velocity range as NGC 4569 and it is not spread on a much wider range, reducing the expected signal to noise per channel. We can thus conclude that, if the stripped gas was still in its neutral phase, we should detect it.

An independent estimate of the upper limit to the column density of the neutral gas in the tail can be inferred using the deep *Herschel* observations shown in Fig. 10. Taking into consideration the typical sky noise level at 250 μm around NGC 4569, given in Ciesla et al. (2012) ($\simeq$0.25 mJy pixel^{-2} corresponding to $\simeq$0.07 mJy arcsec^{-2}), we can derive the detection limit in dust column density using a modified black body emission with $\beta = 2$ and a grain emissivity parameter $k_{250} = 2.0$ cm^2 g^{-1} (e.g. Boselli 2011). This limit can be transformed into a limit in gas column density using a typical gas-to-dust ratio. The gas-to-dust ratio of nearby massive galaxies ranges from 160 (Sodroski et al. 1994) to 70 (Sandstrom et al. 2013). With these values, the detection limit in the gas column density that was derived from 250 μm data should be $\sim 2-5 \times 10^{19}$ cm^{-2}, comparable to the limits of the VIVA survey.

There are other indications that suggest that the gas is ionized within the tail. We can calculate the typical timescale necessary for the ionized gas in the tail to recombine using the relation

$$\tau_{\rm rec} = \frac{1}{n_{\rm e} \alpha_{\rm A}}, \quad (5)$$

where $\alpha_{\rm A}$ is the total recombination coefficient ($\alpha_{\rm A} = 4.2 \times 10^{-13}$ cm^3 s^{-1}; Osterbrock & Ferland 2006). For a typical density of $n_{\rm e} \simeq 2-4 \times 10^{-2}$ cm^{-3}, the recombination time is $\simeq$2 Myr, a short time when compared to the time necessary to produce a tail $\simeq$145 kpc long (see Sect. 4). It is thus conceivable that the gas is kept ionized within the tail. A comparison of the Hα+[NII] frame and the optical and UV images in Figs. 7−9 shows the lack of any compact star-forming region within the tail, ruling out in situ stellar photoionization. The detailed comparison of the ionization models with the spectroscopy properties of the gas in the tail of ESO 137-001 suggests that the gas is not only photoionized by the UV radiation emitted by young stars, but also by other mechanisms. These might be ionization by the hot gas of the intracluster medium, thermal conduction, and turbulent mixing, although there is no direct evidence of their presence (Tonnesen et al. 2011; Fossati et al. 2016). The lack of any star-forming region in the tail, on the contrary present in ESO 137-001 (Jachym et al. 2014), suggests that the contribution of these other mechanisms must be even dominant in NGC 4569.

The lack of star-forming regions in the tail of NGC 4569 may have resulted from two main effects as indicated by the simulations of Tonnesen & Bryan (2012; see also Roediger et al. 2014). The efficiency with which the gas is transformed into stars in the tails of ram pressure stripped galaxies depends on the way the low-density gas cools and condenses in the turbulent wakes. This process is more efficient whenever the density of the intracluster medium is high as in the case of massive clusters, such as Coma and A1367, where most of the tails of stripped material

[6] The HI-deficiency parameter is defined as the difference in logarithmic scale between the expected and the observed HI mass of a galaxy of given angular size and morphological type (Haynes & Giovanelli 1984).

harbour star- forming regions (Yoshida et al. 2008; Yagi et al. 2010; Fossati et al. 2012). The typical density of the intracluster medium in Virgo is ∼a factor of 10 lower than in Coma and A1367 (Briel et al. 1992; Böhringer et al. 1994). By considering a β-model (Cavaliere & Fusco-Femiano 1976) to trace the deprojected distribution of the X-ray emitting gas within Virgo

$$\rho = \rho_0 \left[1 + \left(\frac{r}{r_c}\right)^2\right]^{-\frac{3}{2}\beta}, \quad (6)$$

and assuming a central density of the intergalactic medium of $\rho_0 = 2 \times 10^{-3}$ cm^{-3} (Böhringer et al. 1994), a core radius $r_c = 2.7$ arcmin, and $\beta = 0.47$ (Schindler et al. 1999), we estimate that the density of the intracluster medium near NGC 4569 is $\rho \simeq 10^{-5}$ cm^{-3} (we assume a distance r from the cluster core of 1.7 degrees, corresponding to 0.32 R_{vir}). This value can be compared to the density of the gas used in the simulation of Tonnesen & Bryan (2012), $\rho = 5 \times 10^{-5}$ cm^{-3} for a galaxy of stellar mass 10^{11} $M_\odot$ (vs. $M_{star} = 3 \times 10^{10}$ $M_\odot$ for NGC 4569). The simulations of Tonnesen & Bryan (2012) also indicate that for the star formation to take place in the tail requires a sufficient amount of time (∼200 Myr) for the gas to cool and collapse. This timescale is comparable to the derived age of the interaction (100−300 Myr; Vollmer et al. 2004, Boselli et al. 2006; Crowl & Kenney 2008). It is thus possible that the stripped gas still did not have time to collapse and form new stars. We should recall, however, that these condensed regions of star formation appear in the simulations whenever the gas is allowed to cool and the contribution of the different heating processes is underestimated. The presence of several condensed regions in another Virgo cluster galaxy, IC 3418 (Hester et al. 2010; Fumagalli et al. 2011; Kenney et al. 2014), where the conditions of the intracluster medium are expected to be similar to those encountered by NGC 4569, clearly indicates that the process of formation of these extraplanar HII regions is still far from being understood.

6.4. The evolution of NGC 4569 in the cluster

The new set of extremely deep Hα+[NII] imaging data collected in this work, combined with those available at other frequencies, and the comparison with model predictions allow us to reconstruct the evolution of the galaxy within the Virgo cluster environment. All observational evidence collected so far suggests that NGC 4569 underwent a recent ram pressure stripping event. Given the presence of a nearby companion, IC 3583, at a projected distance of ∼6 arcmin, however, we cannot exclude gravitational perturbations. A gravitational interaction between the two objects, however, seems ruled out by the fact that their most accurate distance estimate, which was performed using the tip of the red giant branch in HST observations, locates IC 3583 in the foreground of the cluster ($D = 9.52$ Mpc) and NGC 4569 at $D \gtrsim 17$ Mpc (Karachentsev et al. 2014). To quantify the importance of any possible tidal interaction with that galaxy we can estimate the duration of a possible tidal encounter between the two galaxies using the relation (Binney & Tremaine 1987)

$$t_{enc} \simeq max[r_{NGC\ 4569}, r_{IC\ 3583}, b]/\Delta V, \quad (7)$$

where $r_{NGC\ 4569}$ (22.8 kpc) and $r_{IC\ 3583}$ (6.9 kpc) are the radii of the two galaxies, b their separation, and ΔV their relative velocity. If we assume that both galaxies are at the same distance, i.e. that $b \simeq 32$ kpc, we can calculate t_{enc} using Eq. (7). IC 3583 has a radial velocity of 1120 km s^{-1}, significantly different from that of NGC 4569 ($vel = -221$ km s^{-1}), thus $t_{enc} \simeq 23$ Myr. This timescale is very short compared to the time required for NGC 4569 to make a complete revolution (≃370 Myr). Although an interaction on their extended halos is still possible, it is quite unlikely that on such a short timescale the tidal interaction is able to remove $\simeq 1.9 \times 10^{10}$ $M_\odot$ of atomic gas.

We can also estimate the typical truncation radius for two interacting galaxies using the relation (Read et al. 2006)

$$r_t \simeq b \left[\frac{m}{M(3+e)}\right]^{1/3}, \quad (8)$$

where m and M are the masses of the two interacting galaxies, b their separation, and e the ellipticity of their orbit. Again assuming $b = 32$ kpc as a lower limit, an ellipticity of $e = 1$ and a stellar mass $M_{star} = 3 \times 10^{10}$ $M_\odot$ for NGC 4569 and $M_{star} = 6.3 \times 10^8$ $M_\odot$ for IC 3583 we obtain a truncation radius $r_t \gtrsim 74$ kpc for NGC 4569 and 5.5 kpc for IC 3583. Since the truncation radius of NGC 4569 is significantly larger than the optical radius (22.8 kpc), it is thus very unlikely that gravitational interactions have been the dominant perturbing mechanism that have affected the recent evolution of that galaxy. This result is consistent with the fact that we do not observe any significant stellar tidal feature that is associated with the observed tails of ionised gas (Fig. 7). We cannot, however, exclude that a fly-by encounter of the two galaxies has occurred. This kind of encounter generally induces nuclear gas infall (Moore et al. 1998). If this did happen, it could explain the prodigious nuclear starburst activity that occurred 3−6 Myr ago (Barth & Shields 2000; Grebel & Bruhweiler 2002), or an older (>15 Myr) starburst (Keel 1996), with possible feeding of a mild nuclear activity. The spectacular optical images, obtained at the CFHT as part of the NGVS survey (Fig. 8), indicate small (a few kpc) low surface-brightness features that are perpendicular to the disc on the south east side of the galaxy or on the north suggesting a possible bridge with IC 3583. A minor gravitational interaction might also have contributed flattening the potential well of the two galaxies, weakening their gravitational binding forces, which keep the diffuse gas of the ISM anchored to the stellar disc, thus making ram pressure stripping more efficient (Gavazzi et al. 2001).

Further evidence of a ram pressure stripping event is the presence of a polarised radio ridge, southwest of the galaxy centre, which was probably produced by a local compression of the gas that was able to organise the magnetic field (Wezgowiec et al. 2012). This polarised radio continuum feature is located south of the main spur of ionized gas coming out from the nucleus of the galaxy. The position of the tails of ionized gas suggests a slightly different orbit to the one proposed by Vollmer (2009), where the galaxy is expected to have crossed the cluster core ∼300 Myr ago and is now coming towards us on a south-west to north-east orbit. Instead, the observed tails of Hα+[NII] gas indicate a west-to-east orbit, putting in question the interpretation of the X-ray distribution of the hot gas in a Mach cone as proposed by Wezgowiec et al. (2011).

The first interesting result of this work is that ram pressure stripping can be the dominant mechanism for removing the ISM in massive galaxies ($M_{star} \simeq 3 \times 10^{10}$ $M_\odot$) that fall into intermediate class clusters ($M_{virial} = 1.4$−4.2×10^{14} $M_\odot$, McLaughlin 1999; Urban et al. 2011; Nulsen & Bohringer 1995; Schindler et al. 1999; $\Delta_{vel} = 800$ km s^{-1}, Boselli et al. 2014a; $\rho_0 = 2 \times 10^{-3}$ cm^{-3} $T = 2.3$ keV, Bohringer et al. 1994), thus extending previous finding to a much broader range of environments and objects (see also Catinella et al. 2013). The galaxy has probably fallen into the cluster from behind, as indicated

by its negative recessional velocity. The tail orientaion indicates that its orbit is from west to east. The galaxy has thus encountered the maximal density of the intracluster gas north to M 87, at a radial distance of $\gtrsim$230 kpc ($\simeq$0.1 $R_{\rm vir}$), where the density of the intergalactic medium is $\rho_{230\ \rm kpc} \simeq 4 \times 10^{-5}$ cm^{-3} as derived using Eq. (4). It is worth mentioning that NGC 4569 is not an isolated case of a massive galaxy with tails of gas that are witnessing an ongoing ram pressure stripping event in the Virgo cluster: NGC 4388 is another obvious candidate (Yoshida et al. 2002; Oosterloo & van Gorkom 2005; Kenney et al. 2008), as well as the seven massive spirals with HI tails that have been observed by Chung et al. (2007).

This analysis also shows that the diffuse component of the ionised gas in the extended tail is a factor of ~90 larger than that expelled by the nuclear outflow. Since the ionized gas is the dominant phase in the tail (the mass of hot gas in the galaxy halo that has been derived from X-ray data is $\lesssim 2 \times 10^8$ $M_\odot$; Wezgowiec et al. 2011), this indicates that in massive galaxies the contribution of the nuclear feedback to the ejection of the gas mass is minimal. Furthermore it can hardly have reproduced the truncated disc in the gas and dust components observed in NGC 4569 and in most of the gas-deficient cluster galaxies with a quenched activity of star formation (Cortese et al. 2012a; Boselli et al. 2014c). As suggested by hydrodynamic cosmological simulations, however, it could have contributed to making the ram pressure stripping efficient by injecting kinetic energy into the ISM (Bahe & McCarthy 2015). The question is whether NGC 4569 is representative of typical massive galaxies in terms of nuclear activity. It is classified as a LINER/HII region transition-type nucleus by Gabel & Bruhweiler (2002). It is also classified as a strong AGN using the BPT diagram (Baldwin et al. 1981), as are 17% of the *Herschel* Reference Survey late-type galaxies with a stellar mass $M_{\rm star} > 10^{10}$ $M_\odot$ (Gavazzi et al., in prep.), and can thus be considered as a typical active massive galaxy. The feedback process that follows the removal of the hot X-ray halo of galaxies that fall in high-density environments in a starvation scenario (Larson et al. 1980) does not seem to be as efficient as cosmological simulations or semi-analytic models indicate (Weinmann et al. 2006; McCarthy et al. 2008, 2011; Font et al. 2008; Kang & van den Bosch 2008; McGee et al. 2009; Kimm et al. 2009; Guo et al. 2011; De Lucia et al. 2012; Bahe & McCarthy 2015). A more realistic description of the (nuclear) feedback process should be considered. Our results provide further evidence that ram pressure is a compelling mechanism for explaining the stripping of the cold gas component of the ISM and thus the quenching of the star formation activity of late-type galaxies in high-density environments.

7. Conclusion

We present new deep, narrow-band Hα+[NII] imaging data of NGC 4569 that has been obtained with MegaCam at the CFHT. The Hα+[NII] image shows the presence of long, low surface-brightness (Σ(Hα + [NII]) $\simeq$ 10^{-18} erg s^{-1} cm^{-2} arcsec^{-2}) tails of ionised gas extending perpendicularly from the disc of the galaxy in a westerly direction of up to $\simeq$145 kpc. The presence of these tails are a clear indication that the galaxy is undergoing a ram pressure stripping event. This observational evidence suggests that the ram pressure stripping mechanism is efficient not only in intermediate-to-low mass galaxies in the core of massive clusters, as was previously thought, but also in massive galaxies located in an unrelaxed cluster of intermediate mass (~10^{14} $M_\odot$) still in formation, with characteristics similar to those encountered in high-density regions at high redshift. The Hα+[NII] image also shows a plume of ionized gas extending $\simeq$8 kpc perpendicular to the nucleus powered by a nuclear outflow. The total mass of the ionized gas in the tail is an important fraction of that of the cold atomic hydrogen that the galaxy has lost during its crossing of the cluster. The mass of the ionized gas expelled by the nuclear outflow, on the contrary, is $\simeq$1% of the total mass of the ionized gas in the tail. It can hardly be at the origin of the truncated gaseous, dust, and star-forming disc of NGC 4569. If we consider NGC 4569 representative of massive galaxies in intermediate density regions, this analysis suggests that ram pressure stripping is the dominant process responsible for the gas removal and for the quenching of the star formation activity that can be observed in galaxies located in high-density regions. The contribution of the nuclear feedback, which is made efficient after the removal of the hot gas halo (starvation), is only marginal and significantly less important than what it is generally assumed in cosmological simulations.

The lack of HII regions, the derived density, and the physical extension of the tails leads us to speculate that the gas is mainly excited by mechanisms other than photoionization. These could be shocks in the turbulent gas, MHD waves, and heat conduction. The presence of thin filamentary structures that can be observed along the tails, and which were reproduced by the most recent hydrodynamic simulations, suggests that magnetic fields might play an important role.

The analysis presented in this work underlines once more how the detailed study of representative objects in the nearby universe, where high-quality multifrequency data and tuned chemo-spectrophotometric and kinematic models are available, is a powerful tool for understanding the environmental mechanisms that affect galaxy evolution. This work is further evidence that deep narrow-band Hα+[NII] imaging obtained with wide-field detectors is probably the most sensitive technique to capture ongoing interactions such as the one observed in NGC 4569. Indeed, at the typical depth that modern instruments can provide, the fraction of galaxies in nearby clusters with tails of stripped material is very small in HI or X-ray, while it strongly increases in Hα. As an example, the number of galaxies with HI tails in the VIVA survey of the Virgo cluster is only seven out of the 53 observed objects. By way of comparison, ~50% of the late-type galaxies observed with a narrow band Hα+[NII] filter in Coma and A1367 by Yagi, Yoshida, and collaborators have extended tails of ionized gas (e.g. Boselli & Gavazzi 2014). The very nature of the physical process that is responsible for the stripping of the gas (ram pressure vs. tidal interactions), for its excitation in the tails or in the plume associated with the nuclear outflow, and for the possible formation of HII regions far from the galactic disc, however, requires deep high-velocity and angular resolution integral field spectroscopic observations that only instruments such as MUSE can provide.

Acknowledgements. This research has been financed by the French ANR grant VIRAGE and the French national program PNCG. We wish to thank the GALEX Time Allocation Committee for the generous allocation of time devoted to this project and B. Poggianti, I. Karachentsev, A. Barth and the anonymous referee for constructive comments. M. Fossati acknowledges the support of the Deutsche Forschungsgemeinschaft via Project ID 3871/1-1. L.C. acknowledges financial support from the Australian Research Council (DP150101734). M. Fumagalli acknowledges support by the Science and Technology Facilities Council [grant number ST/L00075X/1]. E. Toloba is supported by the NSF grant AST-1412504. This research has made use of the NASA/IPAC Extragalactic Database (NED) which is operated by the Jet Propulsion Laboratory, California Institute of Technology, under contract with the National Aeronautics and Space Administration and of the GOLDMine database (http://goldmine.mib.infn.it/) (Gavazzi et al. 2003).

References

Abell, G. O. 1965, ARA&A, 3, 1
Abramson, A., & Kenney, J. D. P. 2014, AJ, 147, 63
Abramson, A., Kenney, J. D. P., Crowl, H. H., et al. 2011, AJ, 141, 164
Alam, S., Albareti, F. D., Allende Prieto, C., et al. 2015, ApJS, 219, 12
Allen, M. G., Groves, B. A., Dopita, M. A., Sutherland, R. S., & Kewley, L. J. 2008, ApJS, 178, 20
Arrigoni Battaia, F., Gavazzi, G., Fumagalli, M., et al. 2012, A&A, 543, A112
Bahé, Y. M., & McCarthy, I. G. 2015, MNRAS, 447, 969
Baldwin, J. A., Phillips, M. M., & Terlevich, R. 1981, PASP, 93, 5
Barth, A. J., & Shields, J. C. 2000, PASP, 112, 753
Barth, A. J., Ho, L. C., Filippenko, A. V., & Sargent, W. L. W. 1998, ApJ, 496, 133
Binggeli, B., Sandage, A., & Tammann, G. A. 1988, ARA&A, 26, 509
Binggeli, B., Popescu, C. C., & Tammann, G. A. 1993, A&AS, 98, 275
Böhringer, H., Briel, U. G., Schwarz, R. A., et al. 1994, Nature, 368, 828
Boselli, A. 2011, A Panchromatic View of Galaxies (Berlin: Wiley-VCH)
Boselli, A., & Gavazzi, G. 2002, A&A, 386, 124
Boselli, A., & Gavazzi, G. 2006, PASP, 118, 517
Boselli, A., Lequeux, J., & Gavazzi, G. 2002, A&A, 384, 33
Boselli, A., Sauvage, M., Lequeux, J., Donati, A., & Gavazzi, G. 2003, A&A, 406, 867
Boselli, A., Boissier, S., Cortese, L., et al. 2005, ApJ, 623, L13
Boselli, A., Boissier, S., Cortese, L., et al. 2006, ApJ, 651, 811
Boselli, A., Boissier, S., Cortese, L., & Gavazzi, G. 2008a, ApJ, 674, 742
Boselli, A., Boissier, S., Cortese, L., & Gavazzi, G. 2008b, A&A, 489, 1015
Boselli, A., Boissier, S., Cortese, L., et al. 2009, ApJ, 706, 1527
Boselli, A., Eales, S., Cortese, L., et al. 2010, PASP, 122, 261
Boselli, A., Boissier, S., Heinis, S., et al. 2011, A&A, 528, A107
Boselli, A., Hughes, T. M., Cortese, L., Gavazzi, G., & Buat, V. 2013, A&A, 550, A114
Boselli, A., Voyer, E., Boissier, S., et al. 2014a, A&A, 570, AA69
Boselli, A., Cortese, L., & Boquien, M. 2014b, A&A, 564, A65
Boselli, A., Cortese, L., Boquien, M., et al. 2014c, A&A, 564, A67
Boselli, A., Fossati, M., Gavazzi, G., et al. 2015, A&A, 579, A102
Briel, U. G., Henry, J. P., & Boehringer, H. 1992, A&A, 259, L31
Byrd, G., & Valtonen, M. 1990, ApJ, 350, 89
Catinella, B., Schiminovich, D., Cortese, L., et al. 2013, MNRAS, 436, 34
Cavaliere, A., & Fusco-Femiano, R. 1976, A&A, 49, 137
Cayatte, V., van Gorkom, J. H., Balkowski, C., & Kotanyi, C. 1990, AJ, 100, 604
Cayatte, V., Kotanyi, C., Balkowski, C., & van Gorkom, J. H. 1994, AJ, 107, 1003
Chabrier, G. 2003, PASP, 115, 763
Chemin, L., Balkowski, C., Cayatte, V., et al. 2006, MNRAS, 366, 812
Chung, A., van Gorkom, J. H., Kenney, J. D. P., & Vollmer, B. 2007, ApJ, 659, L115
Chung, A., van Gorkom, J. H., Kenney, J. D. P., Crowl, H., & Vollmer, B. 2009, AJ, 138, 1741
Chyży, K. T., Soida, M., Bomans, D. J., et al. 2006, A&A, 447, 465
Ciesla, L., Boselli, A., Smith, M. W. L., et al. 2012, A&A, 543, A161
Cortés, J. R., Kenney, J. D. P., & Hardy, E. 2015, ApJS, 216, 9
Cortese, L., Davies, J. I., Pohlen, M., et al. 2010, A&A, 518, L49
Cortese, L., Ciesla, L., Boselli, A., et al. 2012a, A&A, 540, A52
Cortese, L., Boissier, S., Boselli, A., et al. 2012b, A&A, 544, A101
Cortese, L., Fritz, J., Bianchi, S., et al. 2014, MNRAS, 440, 942
Cowie, L. L., & Songaila, A. 1977, Nature, 266, 501
Crowl, H. H., & Kenney, J. D. P. 2008, AJ, 136, 1623
Davies, J. I., Baes, M., Bendo, G. J., et al. 2010, A&A, 518, L48
De Lucia, G. 2011, in Environment and the Formation of Galaxies: 30 Years Later, Astrophys. Space. Sci. Proc., 203
De Lucia, G., Weinmann, S., Poggianti, B. M., Aragón-Salamanca, A., & Zaritsky, D. 2012, MNRAS, 423, 1277
Dressler, A. 1980, ApJ, 236, 351
Dressler, A. 2004, in Clusters of Galaxies: Probes of Cosmological Structure and Galaxy Evolution (CUP), 206
Dressler, A., Oemler, A., Jr., Couch, W. J., et al. 1997, ApJ, 490, 577
Duc, P.-A., Cuillandre, J.-C., Serra, P., et al. 2011, MNRAS, 417, 863
Duc, P.-A., Cuillandre, J.-C., Karabal, E., et al. 2015, MNRAS, 446, 120
Fabian, A. C. 2012, ARA&A, 50, 455
Ferrarese, L., Côté, P., Cuillandre, J.-C., et al. 2012, ApJS, 200, 4
Font, A. S., Bower, R. G., McCarthy, I. G., et al. 2008, MNRAS, 389, 1619
Fossati, M., Gavazzi, G., Boselli, A., & Fumagalli, M. 2012, A&A, 544, A128
Fossati, M., Fumagalli, M., Boselli, A., et al. 2016, MNRAS, 455, 2028
Fumagalli, M., Krumholz, M. R., Prochaska, J. X., Gavazzi, G., & Boselli, A. 2009, ApJ, 697, 1811
Fumagalli, M., Gavazzi, G., Scaramella, R., & Franzetti, P. 2011, A&A, 528, A46
Fumagalli, M., Fossati, M., Hau, G. K. T., et al. 2014, MNRAS, 445, 4335
Gabel, J. R., & Bruhweiler, F. C. 2002, AJ, 124, 737
Gavazzi, G., Catinella, B., Carrasco, L., Boselli, A., & Contursi, A. 1998, AJ, 115, 1745
Gavazzi, G., Boselli, A., Scodeggio, M., Pierini, D., & Belsole, E. 1999, MNRAS, 304, 595
Gavazzi, G., Boselli, A., Mayer, L., et al. 2001, ApJ, 563, L23
Gavazzi, G., Boselli, A., Donati, A., Franzetti, P., & Scodeggio, M. 2003, A&A, 400, 451
Gavazzi, G., Zaccardo, A., Sanvito, G., Boselli, A., & Bonfanti, C. 2004, A&A, 417, 499
Gavazzi, G., O'Neil, K., Boselli, A., & van Driel, W. 2006a, A&A, 449, 929
Gavazzi, G., Boselli, A., Cortese, L., et al. 2006b, A&A, 446, 839
Gavazzi, G., Fumagalli, M., Fossati, M., et al. 2013, A&A, 553, A89
Giovanelli, R., Haynes, M. P., Kent, B. R., et al. 2005, AJ, 130, 2598
Goto, T., Yamauchi, C., Fujita, Y., et al. 2003, MNRAS, 346, 601
Grier, C. J., Mathur, S., Ghosh, H., & Ferrarese, L. 2011, ApJ, 731, 60
Gunn, J. E., & Gott, J. R., III 1972, ApJ, 176, 1
Guo, Q., White, S., Boylan-Kolchin, M., et al. 2011, MNRAS, 413, 101
Haan, S., Schinnerer, E., Mundell, C. G., García-Burillo, S., & Combes, F. 2008, AJ, 135, 232-257
Haines, C. P., Pereira, M. J., Smith, G. P., et al. 2013, ApJ, 775, 126
Haines, C. P., Pereira, M. J., Smith, G. P., et al. 2015, ApJ, 806, 101
Haynes, M. P., & Giovanelli, R. 1984, AJ, 89, 758
Haynes, M. P., Giovanelli, R., Martin, A. M., et al. 2011, AJ, 142, 170
Helfer, T. T., Thornley, M. D., Regan, M. W., et al. 2003, ApJS, 145, 259
Hester, J. A., Seibert, M., Neill, J. D., et al. 2010, ApJ, 716, L14
Ho, L. C., Filippenko, A. V., & Sargent, W. L. W. 1997, ApJS, 112, 315
Hubble, E., & Humason, M. L. 1931, ApJ, 74, 43
Jáchym, P., Combes, F., Cortese, L., Sun, M., & Kenney, J. D. P. 2014, ApJ, 792, 11
Kang, X., & van den Bosch, F. C. 2008, ApJ, 676, L101
Karachentsev, I. D., Tully, R. B., Wu, P.-F., Shaya, E. J., & Dolphin, A. E. 2014, ApJ, 782, 4
Keel, W. C. 1996, PASP, 108, 917
Kenney, J. D. P., van Gorkom, J. H., & Vollmer, B. 2004, AJ, 127, 3361
Kenney, J. D. P., Tal, T., Crowl, H. H., Feldmeier, J., & Jacoby, G. H. 2008, ApJ, 687, L69
Kenney, J. D. P., Geha, M., Jáchym, P., et al. 2014, ApJ, 780, 119
Kennicutt, R. C., Jr. 1983, AJ, 88, 483
Kennicutt, R. C., Jr., & Kent, S. M. 1983, AJ, 88, 1094
Kimm, T., Somerville, R. S., Yi, S. K., et al. 2009, MNRAS, 394, 1131
Koopmann, R. A., Kenney, J. D. P., & Young, J. 2001, ApJS, 135, 125
Larson, R. B., Tinsley, B. M., & Caldwell, C. N. 1980, ApJ, 237, 692
Lewis, I., Balogh, M., De Propris, R., et al. 2002, MNRAS, 334, 673
Maoz, D., Koratkar, A., Shields, J. C., et al. 1998, AJ, 116, 55
Massey, P., Strobel, K., Barnes, J. V., & Anderson, E. 1988, ApJ, 328, 315
McCarthy, I. G., Frenk, C. S., Font, A. S., et al. 2008, MNRAS, 383, 593
McCarthy, I. G., Schaye, J., Bower, R. G., et al. 2011, MNRAS, 412, 1965
McGee, S. L., Balogh, M. L., Bower, R. G., Font, A. S., & McCarthy, I. G. 2009, MNRAS, 400, 937
McLaughlin, D. E. 1999, ApJ, 512, L9
Mei, S., Blakeslee, J. P., Côté, P., et al. 2007, ApJ, 655, 144
Merluzzi, P., Busarello, G., Dopita, M. A., et al. 2013, MNRAS, 429, 1747
Merritt, D. 1983, ApJ, 264, 24
Mihos, J. C., Durrell, P. R., Ferrarese, L., et al. 2015, ApJ, 809, L21
Moore, B., Lake, G., & Katz, N. 1998, ApJ, 495, 139
Nulsen, P. E. J. 1982, MNRAS, 198, 1007
Nulsen, P. E. J., & Bohringer, H. 1995, MNRAS, 274, 1093
Oemler, A., Jr. 1974, ApJ, 194, 1
Oosterloo, T., & van Gorkom, J. 2005, A&A, 437, L19
Osterbrock, D. E., & Ferland, G. J. 2006, Astrophysics of gaseous nebulae and active galactic nuclei (Sausalito, CA: University Science Books)
Read, J. I., Wilkinson, M. I., Evans, N. W., Gilmore, G., & Kleyna, J. T. 2006, MNRAS, 366, 429
Rich, J. A., Kewley, L. J., & Dopita, M. A. 2011, ApJ, 734, 87
Roediger, E., & Brüggen, M. 2007, MNRAS, 380, 1399
Roediger, E., & Brüggen, M. 2008, MNRAS, 388, L89
Roediger, E., & Hensler, G. 2005, A&A, 433, 875
Roediger, E., Brüggen, M., Owers, M. S., Ebeling, H., & Sun, M. 2014, MNRAS, 443, L114
Rubin, V. C., Kenney, J. D., Boss, A. P., & Ford, W. K., Jr. 1989, AJ, 98, 1246
Ruszkowski, M., Brüggen, M., Lee, D., & Shin, M.-S. 2014, ApJ, 784, 75
Sánchez-Gallego, J. R., Knapen, J. H., Wilson, C. D., et al. 2012, MNRAS, 422, 3208

Sandstrom, K. M., Leroy, A. K., Walter, F., et al. 2013, ApJ, 777, 5
Schindler, S., Binggeli, B., & Böhringer, H. 1999, A&A, 343, 420
Scott, T. C., Cortese, L., Brinks, E., et al. 2012, MNRAS, 419, L19
Sodroski, T. J., Bennett, C., Boggess, N., et al. 1994, ApJ, 428, 638
Solanes, J. M., Manrique, A., García-Gómez, C., et al. 2001, ApJ, 548, 97
Spector, O., Finkelman, I., & Brosch, N. 2012, MNRAS, 419, 2156
Storey, P. J., & Zeippen, C. J. 2000, MNRAS, 312, 813
Sun, M., Donahue, M., & Voit, G. M. 2007, ApJ, 671, 190
Sun, M., Donahue, M., Roediger, E., et al. 2010, ApJ, 708, 946
Taranu, D. S., Hudson, M. J., Balogh, M. L., et al. 2014, MNRAS, 440, 1934
Tonnesen, S., & Bryan, G. L. 2009, ApJ, 694, 789
Tonnesen, S., & Bryan, G. L. 2010, ApJ, 709, 1203
Tonnesen, S., & Bryan, G. L. 2012, MNRAS, 422, 1609
Tonnesen, S., & Stone, J. 2014, ApJ, 795, 148
Tonnesen, S., Bryan, G. L., & Chen, R. 2011, ApJ, 731, 98
Tschoeke, D., Bomans, D. J., Hensler, G., & Junkes, N. 2001, A&A, 380, 40
Tüllmann, R., Dettmar, R.-J., Soida, M., Urbanik, M., & Rossa, J. 2000, A&A, 364, L36
Urban, O., Werner, N., Simionescu, A., Allen, S. W., & Böhringer, H. 2011, MNRAS, 414, 2101
Vollmer, B. 2003, A&A, 398, 525
Vollmer, B. 2009, A&A, 502, 427
Vollmer, B., Cayatte, V., Boselli, A., Balkowski, C., & Duschl, W. J. 1999, A&A, 349, 411
Vollmer, B., Marcelin, M., Amram, P., et al. 2000, A&A, 364, 532
Vollmer, B., Cayatte, V., Balkowski, C., & Duschl, W. J. 2001, ApJ, 561, 708
Vollmer, B., Balkowski, C., Cayatte, V., van Driel, W., & Huchtmeier, W. 2004, A&A, 419, 35
Vollmer, B., Huchtmeier, W., & van Driel, W. 2005, A&A, 439, 921
Vollmer, B., Soida, M., Otmianowska-Mazur, K., et al. 2006, A&A, 453, 883
Vollmer, B., Soida, M., Chung, A., et al. 2008a, A&A, 483, 89
Vollmer, B., Braine, J., Pappalardo, C., & Hily-Blant, P. 2008b, A&A, 491, 455
Vollmer, B., Soida, M., Chung, A., et al. 2009, A&A, 496, 669
Vollmer, B., Soida, M., Braine, J., et al. 2012, A&A, 537, A143
Yagi, M., Komiyama, Y., Yoshida, M., et al. 2007, ApJ, 660, 1209
Yagi, M., Yoshida, M., Komiyama, Y., et al. 2010, AJ, 140, 1814
Yagi, M., Gu, L., Fujita, Y., et al. 2013, ApJ, 778, 91
Yoshida, M., Yagi, M., Okamura, S., et al. 2002, ApJ, 567, 118
Yoshida, M., Yagi, M., Komiyama, Y., et al. 2008, ApJ, 688, 918
Yoshida, M., Yagi, M., Komiyama, Y., et al. 2012, ApJ, 749, 43
Young, J. S., Allen, L., Kenney, J. D. P., Lesser, A., & Rownd, B. 1996, AJ, 112, 1903
Weinmann, S. M., van den Bosch, F. C., Yang, X., et al. 2006, MNRAS, 372, 1161
Weinmann, S. M., Kauffmann, G., von der Linden, A., & De Lucia, G. 2010, MNRAS, 406, 2249
Weinmann, S. M., Lisker, T., Guo, Q., Meyer, H. T., & Janz, J. 2011, MNRAS, 416, 1197
Wetzel, A. R., Tinker, J. L., & Conroy, C. 2012, MNRAS, 424, 232
Wetzel, A. R., Tinker, J. L., Conroy, C., & van den Bosch, F. C. 2013, MNRAS, 432, 336
Weżgowiec, M., Vollmer, B., Ehle, M., et al. 2011, A&A, 531, A44
Weżgowiec, M., Bomans, D. J., Ehle, M., et al. 2012, A&A, 544, A99
Whitmore, B. C., Gilmore, D. M., & Jones, C. 1993, ApJ, 407, 489
Zibetti, S., Charlot, S., & Rix, H.-W. 2009, MNRAS, 400, 1181